Earth Syst. Dynam., 13, 1167–1196, 2022
https://doi.org/10.5194/esd-13-1167-2022

Earth System Dynamics
Open Access
EGU

Research article

The ExtremeX global climate model experiment: investigating thermodynamic and dynamic processes contributing to weather and climate extremes

Kathrin Wehrli[1], Fei Luo[2,3], Mathias Hauser[1], Hideo Shiogama[4], Daisuke Tokuda[5], Hyungjun Kim[5,6,7], Dim Coumou[2,3], Wilhelm May[8], Philippe Le Sager[3], Frank Selten[3], Olivia Martius[9,10,11], Robert Vautard[12], and Sonia I. Seneviratne[1]

[1]Institute for Atmospheric and Climate Science, Department of Environmental Systems Science, ETH Zurich, Zurich, Switzerland
[2]Institute for Environmental Studies, VU University Amsterdam, Amsterdam, the Netherlands
[3]Royal Netherlands Meteorological Institute (KNMI), De Bilt, the Netherlands
[4]Center for Global Environmental Research, National Institute for Environmental Studies, Tsukuba, Japan
[5]Institute of Industrial Science, University of Tokyo, Tokyo, Japan
[6]Moon Soul Graduate School of Future Strategy, Korea Advanced Institute of Science and Technology, Daejeon, Korea
[7]Department of Civil and Environmental Engineering, Korea Advanced Institute of Science and Technology, Daejeon, Korea
[8]Centre for Environmental and Climate Science (CEC), Lund University, Lund, Sweden
[9]Oeschger Centre for Climate Change Research, University of Bern, Bern, Switzerland
[10]Institute of Geography, University of Bern, Bern, Switzerland
[11]Mobiliar Lab for Natural Risks, University of Bern, Bern, Switzerland
[12]Institut Pierre Simon Laplace, Laboratoire des Sciences du Climat et de l'Environnement (LSCE), Gif sur Yvette, France

Correspondence: Kathrin Wehrli (kathrin.wehrli@env.ethz.ch)

Received: 8 July 2021 – Discussion started: 13 July 2021
Revised: 22 May 2022 – Accepted: 1 June 2022 – Published: 25 August 2022

Abstract. The mechanisms leading to the occurrence of extreme weather and climate events are varied and complex. They generally encompass a combination of dynamic and thermodynamic processes, as well as drivers external to the climate system, such as anthropogenic greenhouse gas emissions and land use change. Here we present the ExtremeX multi-model intercomparison experiment, which was designed to investigate the contribution of dynamic and thermodynamic processes to recent weather and climate extremes. The numerical experiments are performed with three Earth system models: CESM, MIROC, and EC-Earth. They include control experiments with interactive atmosphere and land surface conditions, as well as experiments wherein the atmospheric circulation, soil moisture, or both are constrained using observation-based data. The temporal evolution and magnitude of temperature anomalies during heatwaves are well represented in the experiments with a constrained atmosphere. However, the magnitude of mean climatological biases in temperature and precipitation are not greatly reduced in any of the constrained experiments due to persistent or newly introduced biases. This highlights the importance of error compensations and tuning in the standard model versions. To show one possible application, ExtremeX is used to identify the main drivers of heatwaves and warm spells. The results reveal that both atmospheric circulation patterns and soil moisture conditions substantially contribute to the occurrence of these events. Soil moisture effects are particularly important in the tropics, the monsoon areas, and the Great Plains of the United States, whereas atmospheric circulation effects are major drivers in other midlatitude and high-latitude regions.

Published by Copernicus Publications on behalf of the European Geosciences Union.

1 Introduction

Weather and climate extremes strongly affect society, human health, and ecosystems; therefore, they need to be accurately simulated in numerical weather predictions and climate projections (e.g., Seneviratne et al., 2012). However, substantial biases remain in their representation in weather and climate models (e.g., Angélil et al., 2016; Maraun et al., 2017; Merz et al., 2020; Moon et al., 2018; Wehrli et al., 2018). For climate models used in the fifth phase of the Coupled Model Intercomparison Project (CMIP5), consistent biases can be found across models in the mean climatology of the lower atmosphere and land surface, for example for temperature and precipitation (Flato et al., 2013; Mueller and Seneviratne, 2014). These biases originate to some extent from the representation of the underlying processes driving evapotranspiration at the land surface (Mueller and Seneviratne, 2014), extratropical cyclones (Zappa et al., 2013), or the simulated sea ice and sea surface temperatures (SSTs) (Turner et al., 2013; C. Wang et al., 2014). The difficulties in representing the mean climatology translate to biases in the representation of extreme events and impede their projection into the future. Therefore, an important question in the investigation of changes in extremes in a warming climate is the identification of the respective contribution of thermodynamic (thermal structure, water vapor, precipitation, land–atmosphere interactions) and dynamic (large-scale circulation) processes to their changes in occurrence and intensity (e.g., Pfahl et al., 2017; Shepherd, 2014; Trenberth et al., 2015; Wehrli et al., 2018, 2019; Zappa et al., 2015). Better isolating these contributions would help inform further model development as well as research on the attribution and projection of changes in weather and climate extremes (Vautard et al., 2016).

In the past, the number of record-breaking hot extremes has increased and it is expected to increase further if anthropogenic emissions continue to rise (e.g., Rahmstorf and Coumou, 2011; Shiogama et al., 2016; Power and Delage, 2019). Changes in the frequency, intensity, and duration of various types of extremes can be seen in different regions of the world (e.g., Seneviratne et al., 2012). The most extreme events show the highest sensitivity to climate change (Seneviratne et al., 2014; Sillmann et al., 2013) and new, not yet seen extreme intensities are anticipated. These changes are related to a number of physical processes, their interactions with each other, and their response to climate change.

The processes driving a specific extreme event and their relative importance can be examined in observation-based studies using linear regression (e.g., Arblaster et al., 2014; Wang et al., 2016; Dirmeyer et al., 2021) or forecast sensitivity experiments (e.g., Hope et al., 2016; Petch et al., 2020). In climate model simulations the role of the drivers can be studied by constraining the processes in the ocean, the atmosphere, or at the land surface, which enables the study of drivers in isolation (e.g., Fischer et al., 2007; Hauser et al., 2016; Jaeger and Seneviratne, 2011). Recent work using these methods has shown that both soil moisture and atmospheric circulation play an important role in driving heatwaves (e.g., Dirmeyer et al., 2021; Petch et al., 2020; Suarez-Gutierrez et al., 2020). In this study, we present the new "ExtremeX" multi-model experiment in which, among other possible applications, the contribution of thermodynamic and dynamic processes to recent extreme events can be investigated in three Earth system models (ESMs). The models used in ExtremeX are the Community Earth System Model version 1.2 (CESM1.2), the Model for Interdisciplinary Research on Climate version 5 (MIROC5), and the European Community Earth System Model version 3 (EC-Earth3). The purpose of this study is (1) to introduce the ExtremeX experiments and (2) to apply the introduced framework to study the drivers of heatwaves as well as to identify regions where warm spells are generally dominated by processes at the land surface or by atmospheric circulation.

The ExtremeX experiment builds on the study of Wehrli et al. (2019). This previous study introduced a framework to disentangle the role of the ocean, atmospheric circulation, soil moisture conditions, and recent climate change in extreme events. Therefore, experiments were carried out with prescribed SSTs and sea ice as well as additionally constraining the land surface and/or the atmosphere using observation-based conditions. Atmospheric variability was constrained using a grid-point nudging approach (Jeuken et al., 1996) to relax the horizontal winds toward reanalysis. This nudging approach has been verified for CESM1.2 (Wehrli et al., 2018), also analyzing biases for the nudged vs. non-nudged model climatologies, showing only minor changes to total biases. In Wehrli et al. (2019), soil moisture in the upper soil layers was constrained to control the role of land surface feedback in extreme events. The experiments with atmospheric nudging and/or prescribed soil moisture were then used to study recent heatwaves, highlighting the combined role of dynamics (i.e., atmospheric circulation) and thermodynamics (in that case referring to land–atmosphere interactions) in driving these events.

Here, building further upon the studies with CESM1.2, we present the results of the same experiments but carried out for three ESMs that were each contributed by one of the collaborating modeling groups. The models do not show high interdependence and are thus an optimal selection for a small ensemble (Brunner et al., 2020; Knutti et al., 2013). EC-Earth3 is the most recent of the three models and hence has the highest horizontal and vertical resolution of the three models used here. Since EC-Earth3 was used for CMIP6, it also has the most recent forcing data. Among CMIP5 and CMIP6 models, EC-Earth3 is one of the best-performing models with regard to the representation of atmospheric circulation in the Northern Hemisphere middle to

high latitudes (Brands, 2022; Fernandez-Granja et al., 2021). MIROC5 has contributed to CMIP5 as well as the 1.5°C versus 2.0°C global warming experiments (e.g., Hirsch et al., 2018; Mitchell et al., 2017; Shiogama et al., 2019).

The presented work expands on previous work in Wehrli et al. (2018, 2019) by quantifying biases of the near-surface climatology for different constraining experiments and three models. Near-surface temperature anomalies during four heatwaves evaluated in Wehrli et al. (2019) are compared in the three ESMs of ExtremeX. Additionally, warm spells are examined grid-point-wise to identify the role of the atmosphere and soil moisture for different spell lengths. The research questions asked are the following.

- Are model deficiencies in atmospheric circulation and the land surface contributing to climatological model biases? Are model biases reduced when these processes are constrained?
- Are the ExtremeX ESMs able to reproduce temperature anomalies of past heatwaves when constrained with observation-based data?
- What is the role of the physical climate drivers and climate change for four observed heatwaves?
- What is the relative contribution of the land surface and the atmospheric circulation to warm spells globally, and how do the contributions vary regionally?

The ExtremeX experiments could also be used to examine types of events other than heatwaves. They are suitable for more in-depth analysis of model biases by examining, for example, the atmospheric moisture and heat budgets or the surface energy balance. In Luo et al. (2022) the ExtremeX experiments are used to study the origin of model biases in the anomaly of upper-level winds and near-surface climatology during certain summertime Rossby wave events in the Northern Hemisphere by constructing composites. Other applications have not been tested so far and will be left to explore in future studies.

In Sect. 2, we introduce the experimental design and methods used. In Sect. 3 we describe the three models composing ExtremeX, and in Sect. 4 we evaluate the constraining of the atmospheric circulation and land surface. Then the framework is applied to investigate the contribution of atmospheric circulation patterns vs. soil moisture conditions for selected heatwaves between 2010 and 2015 (Sect. 5.1) and for the occurrence of warm spells (Sect. 5.2). The conclusions and outlook are given in Sect. 6.

2 Design of the model intercomparison project

The ExtremeX experiment was conducted in collaboration with three modeling groups running three ESMs, two of which (CESM and MIROC) were run in the CMIP5 configuration and one (EC-Earth) in the CMIP6 configuration. Five experiments were designed to unravel the source of model biases and to separate the contribution of atmospheric circulation and land surface conditions to extreme events. This is done by constraining the ocean, land surface, and atmosphere using observation-based data. The experiments and methods used are described in the following and overall follow the setup of Wehrli et al. (2019).

2.1 Experimental design

Five experiments are included in ExtremeX. All experiments prescribe SSTs, sea ice cover fraction, and land use (i.e., vegetation) but differ in the simulation of the atmospheric circulation and soil moisture that are either interactive or constrained. See Table 1 for an overview of the experiments. The control experiment (AI_SI: atmosphere interactive, soil interactive) uses the standard setup wherein the atmosphere and soil moisture are both interactive. In the soil moisture experiment (AI_SF: atmosphere interactive, soil forced) the atmosphere is interactive and soil moisture is constrained, and vice versa for the nudging experiment (AF_SI: atmosphere forced, soil interactive), with the latter only used to validate the atmospheric nudging in this study. Finally, in the fully constrained (AF_SF: atmosphere forced, soil forced) and soil moisture climatology (AF_SC: atmosphere forced, soil climatological) experiments both components are constrained by prescribing soil moisture varying over time or prescribing soil moisture using climatological soil moisture (but including the seasonal cycle), respectively.

For each experiment, one or five simulations are initialized in 1979. The ensembles for AI_SI and AI_SF are enlarged from 5 to 100 members for 2009–2015/16. The number of simulation runs for the other experiments (AF_SI, AF_SC and AF_SF) is constant. The small ensembles of five members for AF_SI from MIROC and CESM were used to confirm that variability between the members is highly reduced for winds at the surface by nudging the higher model levels, even though in the ExtremeX setup, winds are unconstrained in the lowest model levels (Sect. 2.2.1, see also Sect. 4 and Fig. A1). The analysis of the simulations starts in 1982 because the first 3 simulation years are regarded as spin-up. Likewise, 2009 is regarded as the spin-up for the additional members to diverge, and therefore analysis of the years 2010–2015/16 is recommended, for example, for event-based analysis of extremes, as is done here.

For the simulations, natural and anthropogenic forcing was used from observation-based data during the observational period and from scenarios thereafter (Sect. 3). The three models choose different scenarios: either Representative Concentration Pathway 8.5 (RCP8.5; van Vuuren et al., 2011) (CESM), RCP4.5 (MIROC), or Shared Socioeconomic Pathway 3-7.0 (SSP3-7.0; Meinshausen et al., 2020) (EC-Earth). The choice between RCP4.5, RCP8.5, and SSP3-7.0 is not expected to affect the results in this study as the scenarios barely differ for the considered time period.

Table 1. Overview of experiments and configuration of the model components. The number of simulation runs for the experiments is given for the two successive simulation periods (1979–2008 and 2009–2015/16) and for the models in this order: CESM1.2, EC-Earth3, MIROC5.

Name	Acronym	Atmosphere	Soil moisture	Ocean	1979–2008	2009–2015/16
Control	AI_SI	interactive	interactive	prescribed	5, 5, 5	100, 100, 100
Soil moisture experiment	AI_SF	interactive	prescribed	prescribed	5, 5, 5	100, 100, 100
Nudging experiment	AF_SI	nudged	interactive	prescribed	5, 1, 5	5, 1, 5
Fully constrained	AF_SF	nudged	prescribed	prescribed	1, 1, 5	1, 1, 5
Soil moisture climatology	AF_SC	nudged	prescribed*	prescribed	1, 1, 5	1, 1, 5

* Soil moisture is prescribed to the 1982–2008 climatology of the reconstructed soil moisture time series.

2.2 Methods

The ocean, land surface, and atmosphere are constrained to follow observation-based data, either time-varying or climatological. All experiments are conducted with SSTs and sea ice concentration prescribed. In the following, the methods to constrain the atmospheric circulation and the land surface are described. We use the term "constraining" to generally refer to the applied method of nudging the atmospheric large-scale circulation and prescribing soil moisture.

2.2.1 Atmospheric circulation nudging

Nudging the atmospheric circulation in a climate model strongly reduces the dynamic variability in a simulation. For ExtremeX, all modeling groups use a grid-point nudging approach (Jeuken et al., 1996) to constrain the atmospheric large-scale circulation by adding a tendency term to the prognostic equations of the zonal and the meridional winds:

$$\frac{\partial U}{\partial t} = \ldots - \frac{K(z)}{\tau}\left(U(x,t) - U_{\text{target}}(x,t)\right). \quad (1)$$

The term on the right-hand side of Eq. (1) is computed from the difference between a reference data set U_{target} and the computed model value (U). It is weighted by a relaxation timescale τ (Kooperman et al., 2012), which controls the strength of the constraint. A very short relaxation timescale means a strong constraint of the dynamics, while a long relaxation timescale allows larger deviations from the reference. The length of the relaxation timescale is chosen such that it does not dominate model physics but guarantees good agreement with the reference data set. All three models use a 6 h relaxation timescale following Kooperman et al. (2012). The reference data are given by 6-hourly wind fields from the ERA-Interim reanalysis (Dee et al., 2011), which are linearly interpolated to the model time step and regridded to the model resolution. At each model time step, the nudging term is used to update the horizontal wind variables. Additionally, a height-dependent weighting $K(z)$ is introduced, enabling a free evolution of the boundary layer, while the nudging strength increases with height and controls the large-scale circulation (mostly above 700 hPa). The exact implementation of the height-dependent profile was chosen by the groups to individually fit their respective models (Fig. 1).

2.2.2 Prescribing soil moisture

Prescribing soil moisture in a climate model enables the isolation of the main effects of land surface conditions and feedback on climate. In an experiment with an interactive atmosphere but prescribed soil moisture (AI_SF), the circulation will adapt to the given land surface conditions, but there is no feedback in the opposite direction. Hence, the land is decoupled from the atmosphere. In the present setup, soil moisture is prescribed to reflect observed conditions, similar to the SST-driven and nudged circulation simulations. However, directly prescribing soil moisture from observations or observation-based products (e.g., reanalyses) in a climate model can lead to inconsistencies due to differences in model climatologies and soil parameterizations (Koster et al., 2009). Instead, soil moisture reconstructions are generated by driving the land surface module of the respective ESM with meteorological fields from reanalysis data (e.g., air temperature, humidity, wind, precipitation, radiation). The generated daily or 6-hourly soil moisture constitutes the model-specific soil moisture reconstruction. This allows soil moisture in the prescription experiments to follow observed-based soil moisture states, while still being in balance with the model climatologies and land model parameterizations. The method to constrain the land model with soil moisture reconstructions is inspired by the approach developed by Hauser et al. (2017b) for CESM. Not all models followed the approach in every aspect, as it was adapted to the respective model and tools available (see details in the individual model descriptions in Sect. 3). The common idea is that the model hydrology is active, but at the end of each time step the modeled soil moisture is replaced with the target soil moisture from the reconstruction.

2.3 Reference data sets

The atmospheric nudging is validated using winds from ERA-Interim (Dee et al., 2011) as a reference. Monthly near-surface temperature is retrieved at 0.5° resolution from the Climatic Research Unit, University of East Anglia (Harris

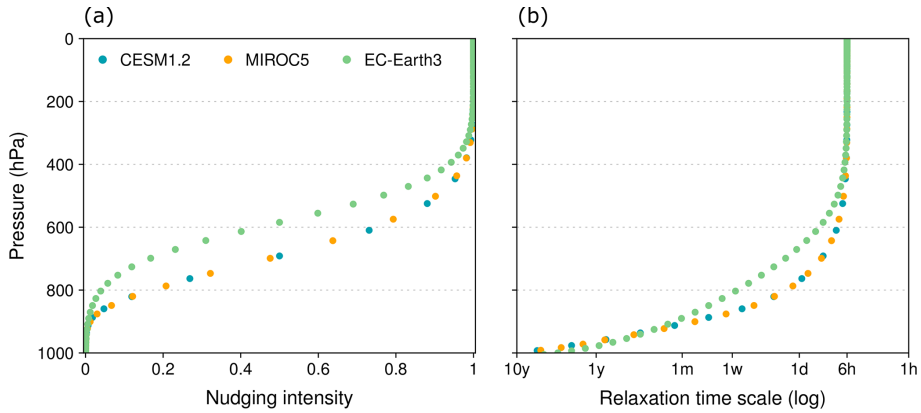

Figure 1. Nudging profile for the three ExtremeX ESMs. The height-dependent nudging intensity ($K(z)$, **a**) and resulting relaxation timescale from the division by τ **(b)** are marked with dots for each model. The nudging intensity is given from zero (no nudging) to 1 (fully nudged).

et al., 2020), using version 4.03 of the data set (CRUTS in the following). Precipitation data at 0.5° resolution are obtained from the Global Precipitation Climatology Centre full data product version 2018 (GPCC-FD; Ziese et al., 2018) and at 0.1° resolution from the Multi-Source Weighted-Ensemble Precipitation data set version 2.2 (MSWEP; Beck et al., 2018). As a reference for evapotranspiration the long, merged synthesis product (based on all data set categories) from the LandFlux-Eval data set at 1° horizontal resolution is used (Mueller et al., 2013). Total cloud cover information was retrieved from the International Satellite Cloud Climatology Project D1 (ISCCP-D1; Rossow and Schiffer, 1999) at 2.5° resolution. All reference data sets are regridded to the original resolution of each model for the comparison.

2.4 Disentangling approach

In Sect. 5, we disentangle the contribution of the physical drivers (atmospheric circulation, land surface conditions, and the ocean state) and of recent climate change to temperature extremes. The method is briefly explained below, and readers can refer to Wehrli et al. (2019) for more details. The disentangling method only takes anomalies of a variable with respect to the experiment climatology into account. In this study, the disentangling is applied to anomalies of daily mean temperature and daily maximum temperature (TX). The different contributions are assumed to be additive, and hence differences between the experiments are computed as shown in Fig. 2.

The fully constrained experiment (AF_SF) is taken as the "model truth" because it is as close to observations as the model can get. Therefore, AF_SF is set to 100 % of the event and the disentangling method determines what fraction of the event anomaly is explained by the other experiments. First, the contribution of recent climate change is computed as the anomaly of the years 2010–2015/16 during the same time of the year the event took place (but excluding the event year) in AI_SI with respect to its 1982–2008 climatology. Note that a small fraction of the 2010–2015/16 anomalies related to the prescribed SST conditions could also be due to decadal variability. The anomaly of AI_SI at a specific point in time (e.g., during an extreme event) compared to its 1982–2008 climatology is a combination of recent climate change (i.e., warming since the climatology period, which is estimated in the first step using the anomaly of non-event years from AI_SI), the observed SST pattern, and natural variability. The natural variability is controlled by using a large ensemble of 100 members. Hence, following the additive assumption, the remaining anomaly of AI_SI corresponds to the contribution of the ocean. To estimate the contribution of the land surface state (i.e., soil moisture) and the atmospheric circulation, the disentangling method by Wehrli et al. (2019) follows two approaches. The first approach (A) is to quantify the contribution of soil moisture as the anomaly in AI_SF minus the anomaly in AI_SI and the contribution of the atmospheric circulation as the anomaly in AF_SF minus the anomaly in AI_SF. The second approach (B) is to quantify the contribution of soil moisture as the anomaly of AF_SF minus the anomaly of AF_SC and the contribution of the atmospheric circulation as the anomaly of AF_SC minus the anomaly of AI_SI. Wehrli et al. (2019) show that the two approaches give similar results, which is confirmed here (Sect. 5). Hence, in this study the results from approaches A and B are averaged, giving equal weight to both. The results for the single approaches are also documented in the Appendix. The individual data analysis carried out for four recent heatwaves in Sect. 5.1 and warm spells in Sect. 5.2 is described in the respective sections.

3 Model descriptions

3.1 Community Earth System Model (CESM)

The Community Earth System Model is run in version 1.2 (CESM1.2; Hurrell et al., 2013). Coupled are the Community Atmosphere Model version 5.3 (CAM5; Neale et al.,

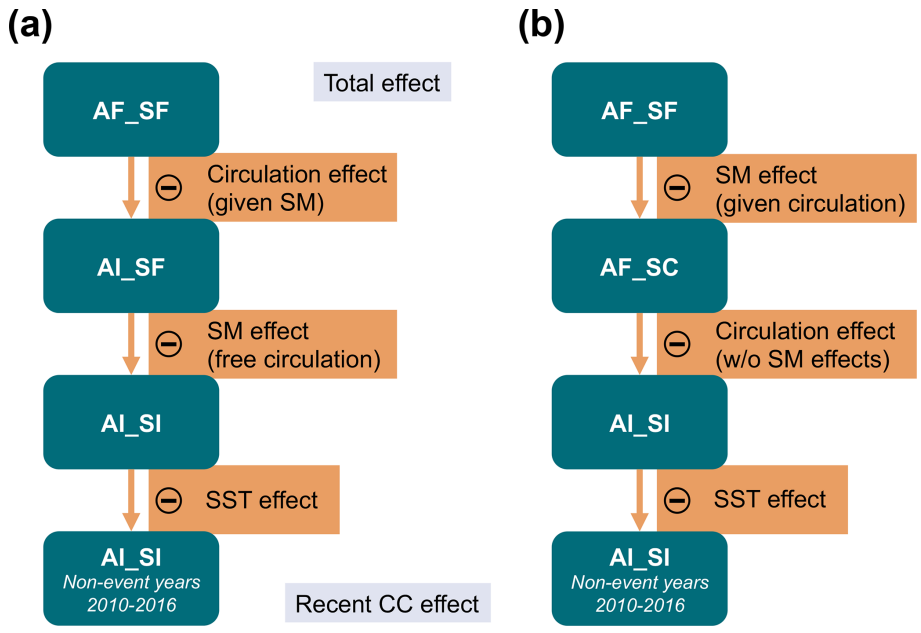

Figure 2. Schematic showing model experiments and effects isolated for extreme temperature events. For the experiments, the anomaly during the event (or during the same time of the year but for non-event years) is considered relative to the 1982–2008 climatology (turquoise rectangles). The magnitude of the anomaly in AF_SF is taken as the total effect, and the anomaly of AI_SI during non-event years is taken as the recent climate change (CC) effect (grey boxes). Further effects are disentangled by computing differences between the experiments along the orange arrows as indicated by the minus sign (orange rectangles). Two approaches (black letters **a** and **b**) are followed, differing in how soil moisture (SM) contributions are separated from atmospheric circulation contributions.

2012) and the Community Land Model version 4 (CLM4; Lawrence et al., 2011; Oleson et al., 2010). Both are run on a horizontal resolution of $0.9° \times 1.25°$. The atmosphere model, CAM5, uses hybrid sigma–pressure coordinates and has 30 vertical layers. CLM4 has 15 soil layers, from which active hydrology is computed in the upper 10 layers (down to 3.8 m).

Natural forcings as well as forcings from greenhouse gases (GHGs), aerosols, and land use change follow the setup in Wehrli et al. (2019). Major GHGs (CO_2, N_2O, and CH_4) are prescribed to observed global values, whereas other anthropogenic forcings follow RCP8.5 after 2005. A merged product of the Hadley Centre sea ice and SST data set version 1 (HadISST1) and the NOAA weekly optimum interpolation SST analysis version 2 (OI2) was used to prescribe transient monthly observations of SSTs and sea ice concentrations (Hurrell et al., 2008). For prescribing soil moisture, the prescription method developed by Hauser et al. (2017b) was used, which replaces the model-calculated soil moisture value by a target value at the end of each model time step. The prescribed target soil moisture is computed by running CLM4 offline driven by reanalysis data from ERA-Interim. Below 0 °C soil temperature in the model, soil moisture is computed interactively, whereas at warmer temperatures the soil liquid water is prescribed to the total (liquid + ice) soil moisture of the target data set. This prevents artificial creation of ice, which can produce unrealistic heat fluxes (Hauser et al., 2017b).

3.2 Model for Interdisciplinary Research on Climate version 5 (MIROC5)

The Model for Interdisciplinary Research on Climate version 5 (MIROC5) was developed jointly at the Atmosphere and Ocean Research Institute (University of Tokyo), the National Institute for Environmental Studies, and the Japan Agency for Marine–Earth Science and Technology (Watanabe et al., 2010). The horizontal spectral resolution of the model is T85 (wave number 85 with triangular truncation corresponding to a horizontal resolution of about 160 km). There are 40 vertical model levels of hybrid sigma–pressure coordinates up to 3 hPa. The land scheme of MIROC5 is an updated version of Minimal Advanced Treatments of Surface Interaction and Runoff (MATSIRO; Takata et al., 2003), which predicts the temperature and water in six soil layers down to a depth of 14 m, one canopy layer, and three snow layers. The SST and sea ice concentration data from HadISST1 were used (Rayner et al., 2003). See Shiogama et al. (2013) for the setup of natural (solar irradiance and volcanic activity) and anthropogenic (GHGs, sulfate, black and organic carbon aerosols, ozone, land use land cover change) forcing agents. The anthropogenic forcing agents after 2005 were based on RCP4.5.

For prescribing soil moisture in MIROC5, the model replaces the calculated soil moisture with a target value at the beginning of each model time step. The prescribed target soil moisture was simulated by the land scheme in offline mode driven by atmospheric fields from ERA-Interim. To remove negative values of liquid soil moisture content, the replacing procedure also limits ice content so that the total soil moisture does not exceed the prescribed one.

3.3 European Community Earth System Model version 3 (EC-Earth3)

The European Community Earth System Model (EC-Earth3) is a climate model with the atmosphere component based on the European Centre for Medium-Range Weather Forecasts (ECMWF) Integrated Forecasting System (IFS), and it is maintained by the EC-Earth consortium. Version 3.3.1 with IFS cycle cy36r4 was used for the ExtremeX experiments. The horizontal spectral resolution of the model is T255 (about 80 km), and there are 91 vertical model levels. The model has a hybrid sigma–pressure coordinate system and a reduced Gaussian grid (N128). All experiments were produced with the SSP3-7.0 CMIP6 scenario and prescribed monthly ocean fields from the merged HadISST1 and NOAA OI2 data set with pre-applied SST and sea ice consistency checks (Hurrell et al., 2008). More information regarding the model can be obtained from https://www.ecmwf.int/ (last access: 26 July 2022), http://www.ec-earth.org/ (last access: 26 July 2022) and Döscher et al. (2022) for greenhouse gases, aerosols, and land use prescribed in EC-Earth3.

For prescribing soil moisture in EC-Earth, the simulated soil moisture is replaced by the respective target values for each of the four soil layers at the end of each model time step. As target values, 6-hourly soil moisture data from ERA-Interim/Land (Balsamo et al., 2015) were used. ERA-Interim/Land uses the H-TESSEL land surface model (Balsamo et al., 2009), which has four soil layers covering 0–7, 7–28, 28–100, and 100–255 cm of the soil.

4 Validation of the constrained atmosphere and soil moisture experiments

In the setup used for this study, the atmospheric nudging is stronger in the upper atmosphere and close to zero at the surface (Fig. 1). Hence, it can be expected that the variability between ensemble members is strongly reduced, especially at higher atmospheric levels, and that the simulated winds closely follow the winds in ERA-Interim with increasing nudging strength. This is confirmed by evaluating the wind fields of the three models at the grid-point level. For MIROC (and less visibly also for CESM; Fig. A1) there is some variability in wind speed and direction between the five members of the AF_SI ensemble at near-surface levels, whereas at 500 hPa and above all members are nearly identical with an almost exact representation of the reference wind speed and direction. For EC-Earth, only one simulation of AF_SI was run. Although the nudging profile of EC-Earth is shifted to higher altitudes compared to the other two models (Fig. 1), the horizontal winds represent the reference equally well for the selected pressure levels (Fig. A1; see also Fig. A2). For all models, nudging the large-scale atmospheric flow also has a strong control on near-surface winds.

In the following, the climatological model biases are compared between the experiments. First, regional and global root mean square errors (RMSEs) are examined in Sect. 4.1. Then, the sign and location of seasonal biases are discussed in Sect. 4.2.

4.1 Global and regional biases in surface temperature and precipitation

Intuitively, one might expect that biases with respect to observations are reduced when soil moisture, atmospheric circulation, or both are constrained. Near-surface temperature, for example, is driven by radiative processes and surface turbulent fluxes. The incoming radiation is related to the abundance, thickness, and composition of clouds, which are parameterized in the models and driven by weather systems (e.g., Bony et al., 2015). Surface turbulent fluxes are driven by soil moisture availability, which affects the partitioning in sensible and latent heat fluxes, especially in transitional climate regimes (e.g., Miralles et al., 2019; Santanello et al., 2018; Seneviratne et al., 2010). Similarly, precipitation is affected by both soil moisture and atmospheric circulation. The location and intensity of rainfall and snow are driven by the passage of low- and high-pressure systems as well as by soil moisture conditions (e.g., van der Ent et al., 2010; Guillod et al., 2015; Moon et al., 2019).

In the following, we quantify the near-surface temperature and precipitation biases in the experiments. Therefore, the model climatologies are compared to a reference by computing the root mean square errors (RMSEs) for the seasonal and annual averages of the 1982–2008 climatology. The mean over all simulation runs was computed when multiple members were available. Only land grid points are considered (except Antarctica).

In the global and annual average, the RMSEs in the experiments with a nudged atmosphere and/or prescribed soil moisture are nearly equal to the RMSE in AI_SI (Fig. 3). For EC-Earth the temperature bias increases when soil moisture is prescribed in AI_SF and AF_SF (Fig. 3a). For MIROC a large precipitation bias is introduced when nudging the atmospheric circulation in AF_SI (Fig. 3b). However, the bias is reduced in the fully constrained experiment (AF_SF). Temperature biases are largest during the December–January–February (DJF) season in CESM and EC-Earth. In MIROC they are largest during the June–July–August (JJA) season, except for AF_SF wherein biases are largest in DJF. Precipitation biases are largest in JJA for all models. For the annual regional averages, large temperature biases can be

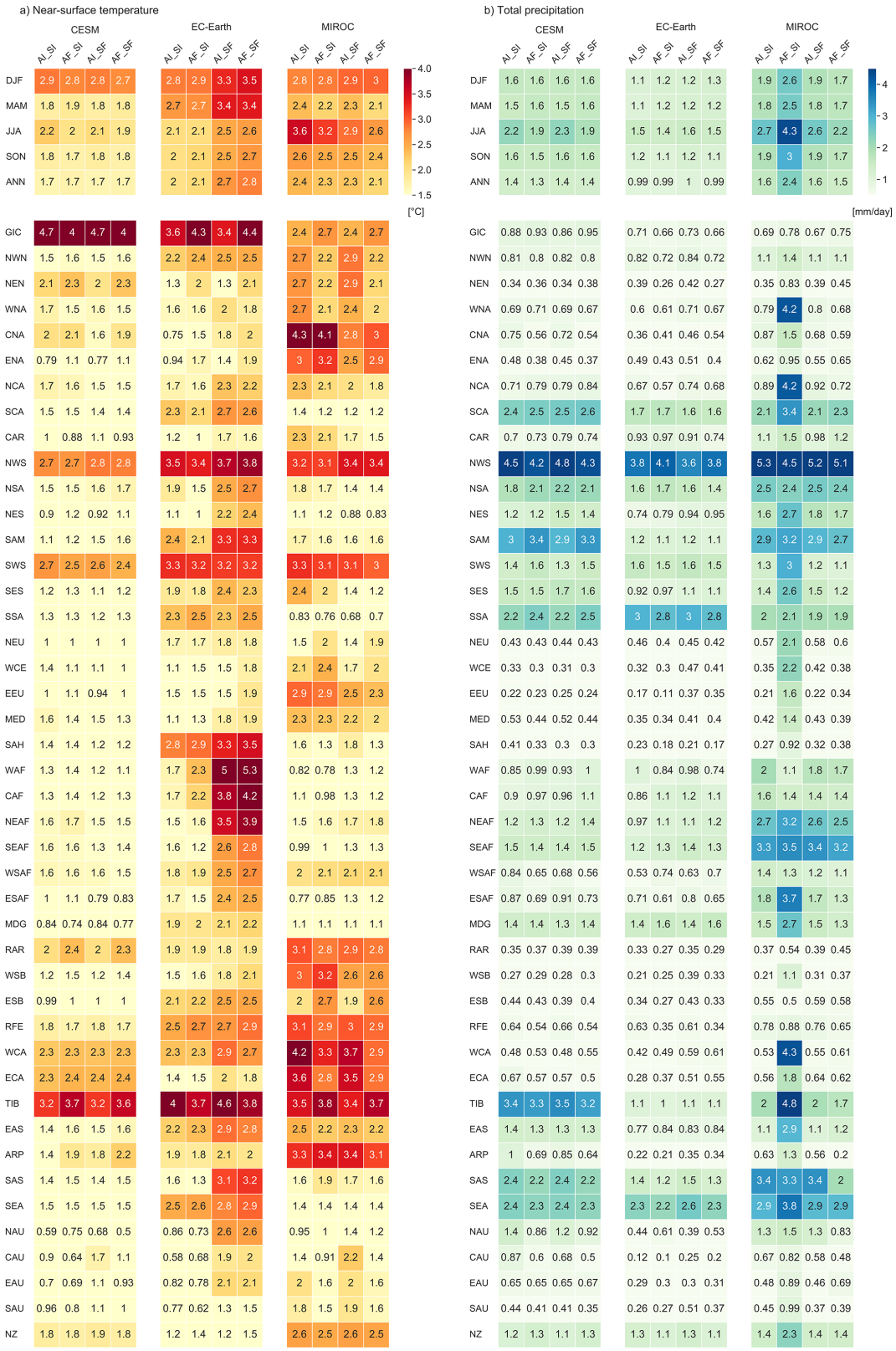

Figure 3. Root mean square errors (RMSEs) for **(a)** near-surface temperature and **(b)** total precipitation. The top section shows the global RMSE for land grid points as well as seasonal and annual (ANN) averages. The bottom section shows the average annual RMSE for the reference regions from the Sixth Assessment Report (AR6) on climate change (Iturbide et al., 2020). For an overview of the AR6 reference regions see Fig. A3. Ocean grid points and Antarctica are excluded.

found in regions with sparse observational coverage such as GIC (Greenland–Iceland), NEN (northeastern North America), and RAR (Russian Arctic; Iturbide et al., 2020, for an overview of the AR6 reference regions see Fig. A3). Large temperature biases can also be found in small regions, which are only represented by a few grid points in the models used, such as NWS (northwestern South America), SWS (southwestern South America), and NZ (New Zealand). Additionally, the complex topography of the Himalayas (TIB) and Andes (SWS and NWS) is also a likely source of temperature biases. Regional precipitation biases are generally larger in wet regions such as the Amazonian regions SAM (South American monsoon) and NSA (northern South America), the regions in central Africa, namely CAF (central Africa), SEAF (southeastern Africa), and NEAF (northeastern Africa), and the monsoon regions SEA (southeastern Asia) and SAS (southern Asia). Precipitation biases are also larger for small regions.

In general, the experiments with a nudged atmosphere and/or prescribed soil moisture do not show a significant reduction of the surface climatology RMSEs in any of the models or for any region of the world. In many cases, constraining the components of the model leads to even larger biases. This contradicts the initial intuitive assumption and suggests that no sole component of the model is responsible for the biases. Hence, the climatological biases that are discussed here cannot be corrected by improving the representation of the model components in isolation.

4.2 Location and sign of seasonal biases

In the Northern Hemisphere midlatitudes, the control simulations (AI_SI) for the CESM and MIROC models are systematically too hot (Fig. 4a) and in some regions also too dry (Fig. 5a) during boreal summer (JJA). North America, central Asia, and eastern Europe show the largest biases. This agrees with the findings by Wehrli et al. (2018) for CESM. For EC-Earth, only central Asia and parts of the midwestern United States (US) are too hot and dry, while other regions are mostly too cold and wet. In all models, the regions where JJA temperature is overestimated coincide with regions where cloud coverage is underestimated (Fig. A4). Especially in MIROC, a large negative cloud cover bias can be found for the Northern Hemisphere midlatitudes. In MIROC, large areas in central and eastern North America, eastern Europe, and Asia show a negative evapotranspiration bias as well (Fig. A5). In CESM and EC-Earth evapotranspiration is underestimated in central Asia and parts of western North America. This indicates that the warm temperature biases are related to underestimated evapotranspiration and cloud coverage in JJA.

Nudging the atmosphere in AF_SI reduces some of the JJA temperature biases in the Northern Hemisphere in CESM and MIROC (Fig. 4a). For MIROC, large precipitation biases are introduced with nudging (Fig. 5a). Some of the midlatitude regions change from too little precipitation to too much and vice versa. Hence, correcting the atmospheric circulation seems to lead to an overcompensation of biases in MIROC. In EC-Earth, nudging does not strongly affect the JJA temperature and precipitation climatology. Constraining the soil moisture in AI_SF leads to a reduction of the hot and dry bias in the Northern Hemisphere midlatitudes in MIROC. For CESM, the changes are smaller but there is a reduction of the hot and dry bias in Europe and the US Midwest. For EC-Earth, constraining the soil moisture, however, introduces or increases the cold and dry bias nearly everywhere. The fully constrained experiment (AF_SF) is the experiment with the smallest temperature and precipitation biases for CESM and MIROC, suggesting that at least for these models, a correct representation of atmospheric circulation patterns and soil moisture conditions can improve the models' overall performance. Nonetheless, for EC-Earth AF_SF shows larger climatological temperature biases than AI_SI (Fig. 4), and for precipitation, the biases remain of similar magnitude (Fig. 5). This indicates that even if some of the temperature and precipitation biases are reduced by constraining the atmospheric circulation and soil moisture in the model using observation-based data, other biases can be enhanced or change sign, resulting in a worse overall performance.

The results for the austral summer (DJF) confirm the findings for the Northern Hemisphere in JJA. For EC-Earth, AI_SF introduces and increases a cold (Fig. 4b) and wet bias (Fig. 5b) in the entire Southern Hemisphere. MIROC shows large precipitation biases for AF_SI, which in certain places are of the opposite sign but of similar or larger magnitude than in AI_SI. For CESM there are only very small differences between the experiments.

All models show substantial biases in total cloud cover fraction (Fig. A4) and evapotranspiration (Fig. A5), which match the biases found in temperature (e.g., negative cloud cover bias and negative evapotranspiration bias for areas that are too warm in the model) and sometimes also for precipitation. Both variables rely heavily on parameterizations. An alternative explanation for why biases are still prevalent after correcting the atmospheric flow and the land surface is that ESMs are tuned to match, e.g., the radiation balance at the top of the atmosphere and global mean values of variables like near-surface temperature, clouds, or sea ice (Mauritsen et al., 2012). When single components of the models are constrained using more realistic fields from observational products, the model components are no longer in balance with each other. This can result in an overcompensation of biases, as can be seen, for example, for precipitation in MIROC (Fig. 5). It is known that MIROC5 shows biases in the North Atlantic storm-track activity compared to ERA-Interim (e.g., Brands, 2022; Zappa et al., 2013). Correcting this circulation bias in AF_SI leads to even larger precipitation biases, which are only reduced when the soil moisture is constrained as well.

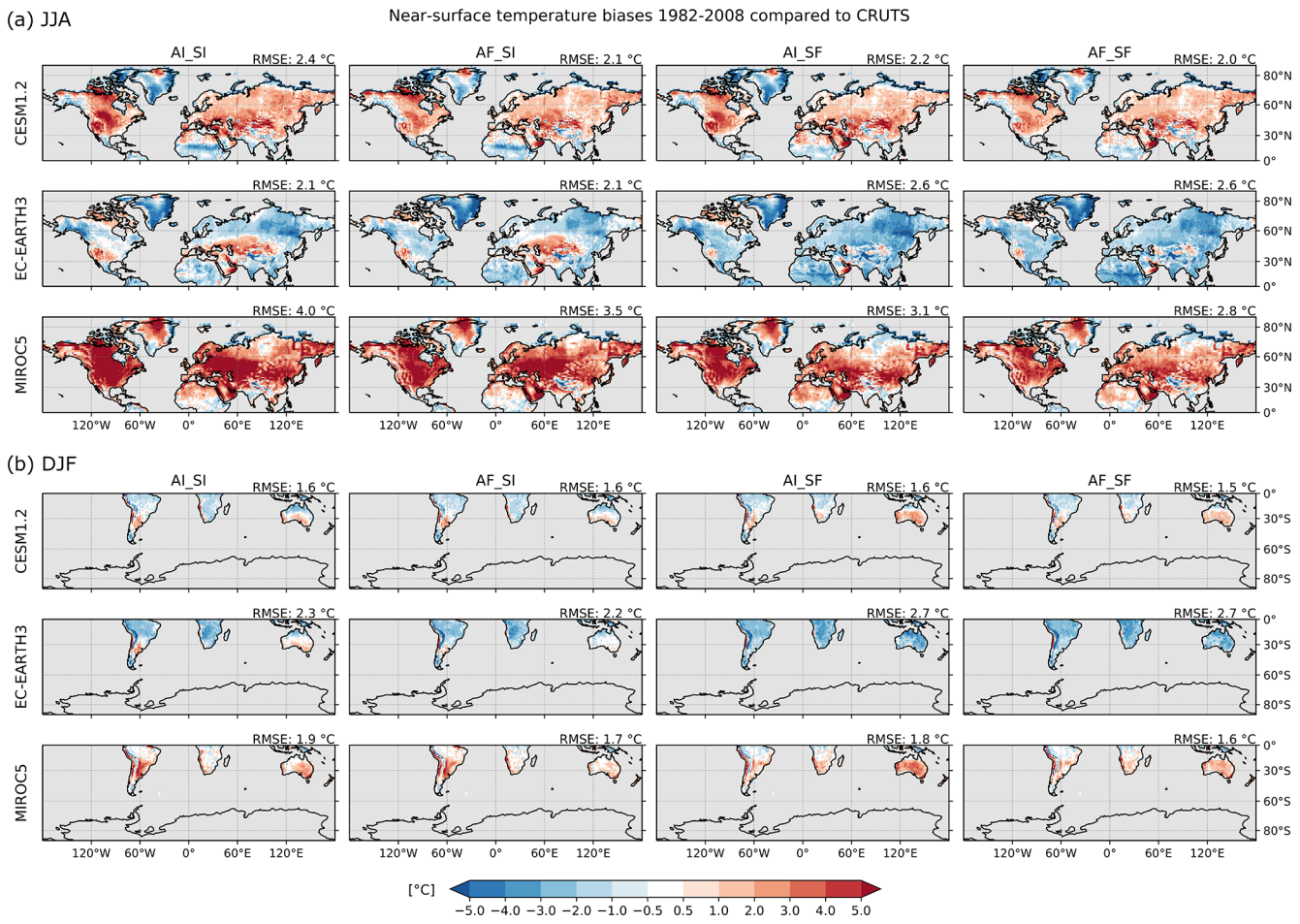

Figure 4. Bias in near-surface temperature (2 m) with respect to CRUTS. Shown is the seasonal average over **(a)** June–July–August (JJA) for the Northern Hemisphere and **(b)** December–January–February (DJF) for the Southern Hemisphere. Ocean grid points and Antarctica are masked out in grey. The root mean square error (RMSE) averaged over all land grid points of the respective hemisphere is given in the upper right corner of each experiment and model.

The seasonal precipitation climatology from the models was also compared to MSWEP (Fig. A6), confirming the above findings. The results for DJF for the Southern Hemisphere are very similar to the biases using GPCC-FD as a reference. For JJA for the Northern Hemisphere, the models are more on the dry side when compared to MSWEP than if GPCC-FD is used as a reference. The hemisphere-averaged RMSEs are in both cases very similar. Overall, the biases are not substantially reduced in any of the models when nudging the atmospheric circulation and/or prescribing soil moisture using observation-driven reconstructions. This shows that model biases are not primarily caused by the misrepresentation of large-scale atmospheric motion or soil moisture conditions. Instead, the biases might be caused by other processes such as radiation and cloud processes, convection, precipitation, land surface properties (e.g., land cover and land use, topography), and processes unresolved due to the model grid scale such as mesoscale circulations and sub-grid surface heterogeneity. The results also suggest that the models are tuned to have low temperature and precipitation biases in the interactive setup (with prescribed ocean).

5 Disentangling the contribution of physical drivers and climate change to recent heatwaves

In the previous section it was shown that large biases remain in the model climatology even if observation-based conditions are used to constrain the models. Nevertheless, nudging the large-scale atmospheric circulation and prescribing the soil moisture results in simulations that can accurately reproduce the temporal evolution and relative magnitude of events. This was shown by Wehrli et al. (2019) using CESM for five recent heatwaves, considering anomalies of TX. Hence, the presented set of experiments can be used to analyze extreme events if anomalies are used or a more elaborate bias-correction method is performed (e.g., Wehrli et al., 2020). In Sect. 5.1, four recent heatwaves are examined, and it is shown that all three models accurately reproduce TX anoma-

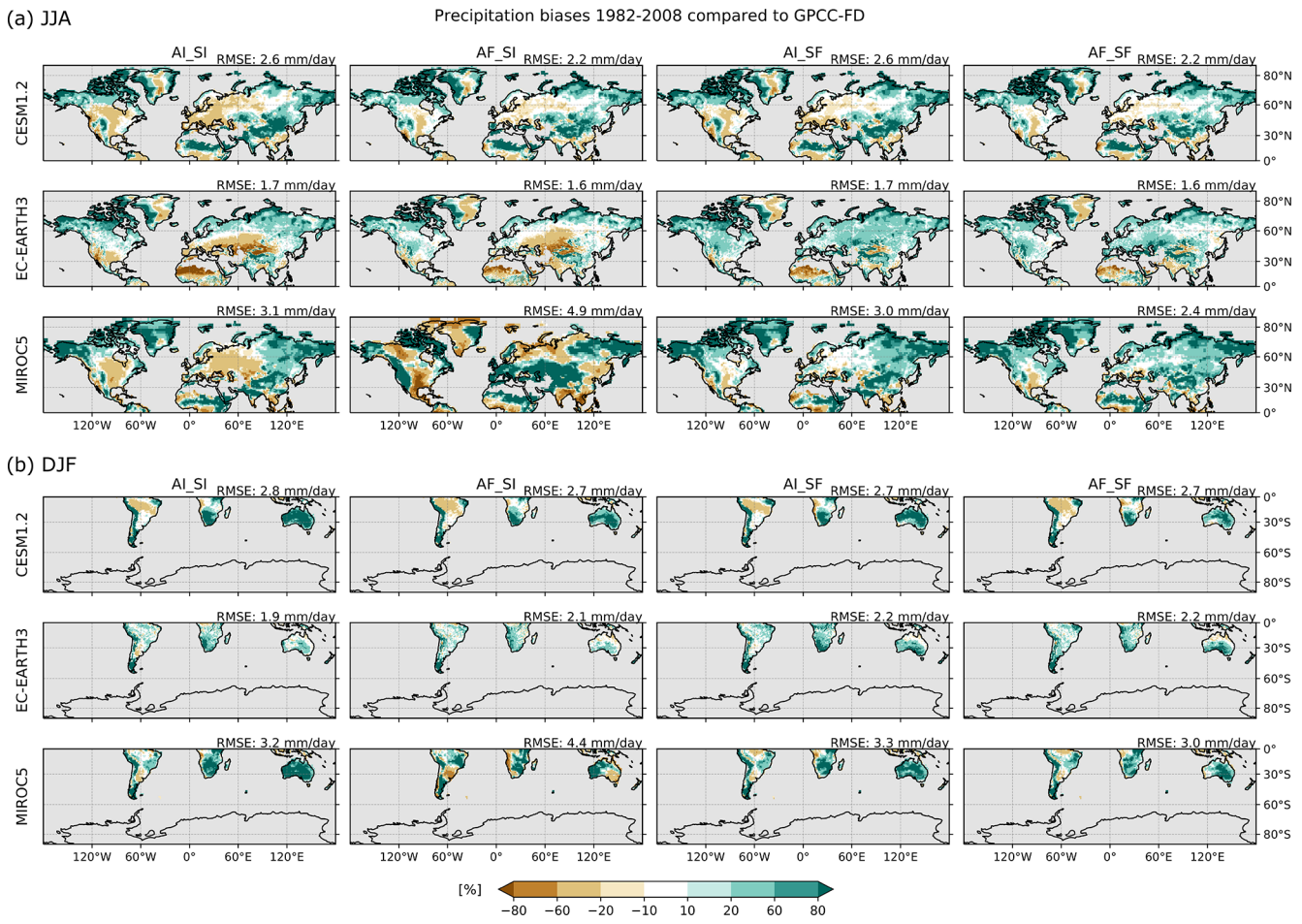

Figure 5. Bias in total precipitation with respect to GPCC-FD. Shown is the seasonal average over **(a)** JJA for the Northern Hemisphere and **(b)** DJF for the Southern Hemisphere. Values are plotted as the percentage deviation from the reference data set. Ocean grid points, Antarctica, and grid points with a seasonal average of less than 0.1 mm precipitation per day in the reference data set are masked out in grey. The RMSE averaged over all valid grid points of the respective hemisphere is given in millimeters per day in the upper right corner of each experiment and model.

lies during and prior to heatwaves when constrained with observation-based data. Then, the contribution of physical drivers and climate change is disentangled for the four heatwaves. The events chosen are the 2010 Russian heatwave, the 2015 European heatwave, the 2012 heatwave in the US (also known as the Midwest heatwave), and the Australian heatwave of 2012/13. All events had drastic consequences for the local communities and economies due to, e.g., damage to agriculture, wildfires, and increased mortality. They were investigated in numerous previous studies including Wehrli et al. (2019). The events were chosen due to their severity and impact as well as to ensure consistency and comparability with Wehrli et al. (2019). In Sect. 5.2 warm spells (during the warm season) are analyzed grid-point-wise to identify the relative contribution of atmospheric circulation vs. soil moisture.

5.1 Driving processes of recent heatwaves

For four heatwaves, the relative contributions of atmospheric circulation, soil moisture, ocean conditions, and climate change (since 1982–2008) to TX anomalies are determined. As in Wehrli et al. (2019), spatial averages are taken over the event region, and daily mean near-surface temperatures from ERA-Interim are used to identify the events. The hottest 15 d period defines the event, and TX during this period is examined. Ocean grid points are excluded from the analysis.

TX anomalies (with respect to 1982–2008) for the heatwaves and previous months are shown in Fig. 6. Overall, the fully constrained experiments (AF_SF) from all models agree well with temperature anomalies from reanalysis and among each other. Small deviations are found during the 2010 Russian heatwave for MIROC, which underestimates the temperature anomaly (Fig. 6a), and during the 2012 US heatwave for which CESM overestimates the

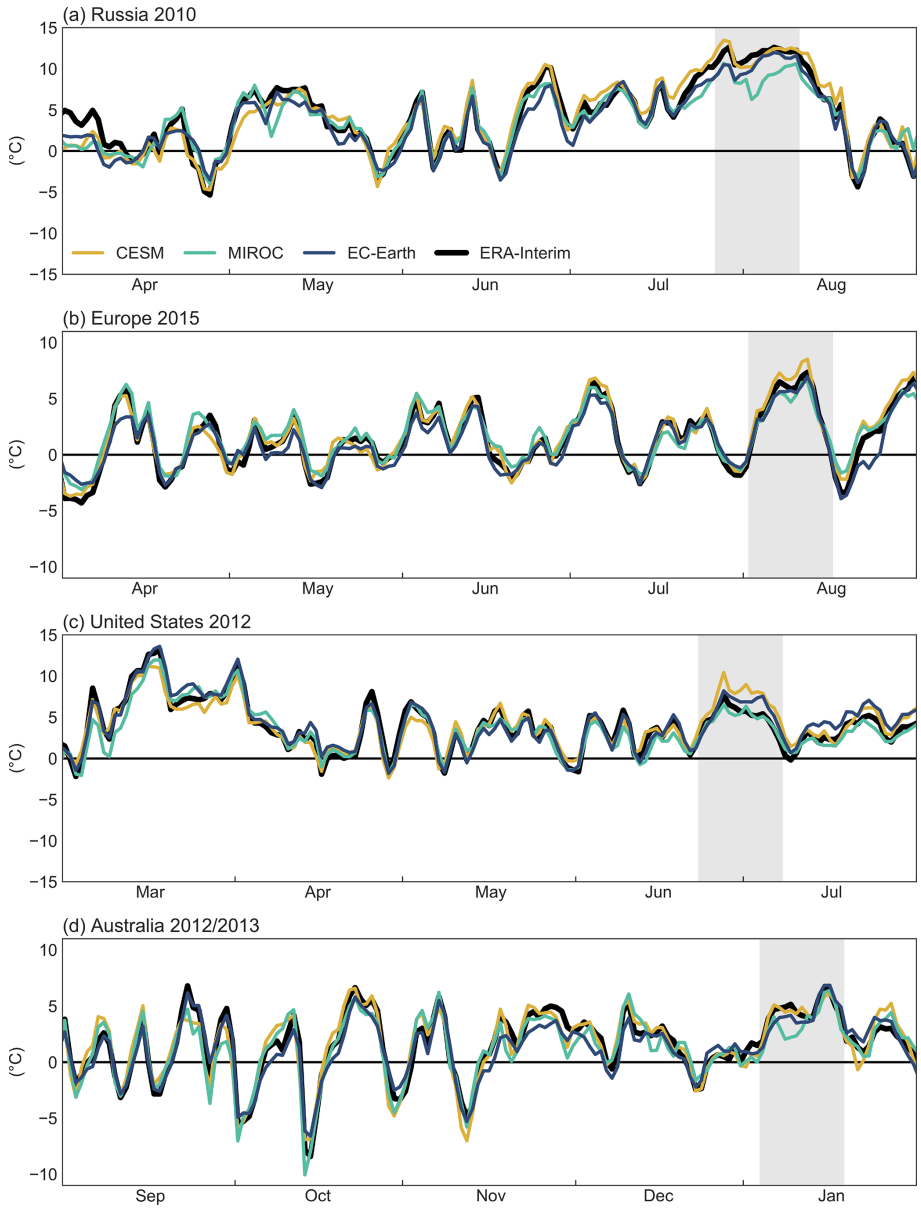

Figure 6. Daily maximum temperature anomaly compared to the 1982–2008 climatology for the fully constrained (AF_SF) experiment for the three models and for ERA-Interim (black line). The 15 d event period is highlighted in light grey.

temperature anomaly (Fig. 6c). TX anomalies for the same events from the nudging experiment (AF_SI) already compare well to ERA-Interim (Fig. A7), capturing the temporal evolution of TX anomalies similarly well as AF_SF. Correlation of near-surface temperature anomalies between the experiments with atmospheric nudging and with ERA-Interim is very high. This confirms that observed surface anomalies can be accurately reproduced when nudging the atmospheric circulation. For MIROC and CESM, which both have five AF_SI simulation runs, it can also be seen that nudging the atmosphere strongly constrains variability between ensemble members (Fig. A7). In the following, the four heatwaves are analyzed separately.

The Russian heatwave of 2010 was characterized by extremely high temperatures over a long time period from late June to mid-August. A persistent blocking anticyclone was associated with the heatwave (e.g., Barriopedro et al., 2011; Trenberth and Fasullo, 2012). Due to early snowmelt in the year and a deficit of precipitation, water scarcity was exacerbating the heatwave (Barriopedro et al., 2011). For the analysis of the Russian heatwave of 2010, regional averages are computed over 50 to 60° N and 35 to 55° E (see Fig. A3 for the region outline). The hottest 15 d period lasts from 27 July

to 10 August 2010 (Fig. 6a). TX anomalies from ERA-Interim exceed 10 °C during the event, which is captured well by CESM and EC-Earth. In MIROC the anomaly is somewhat weaker. In general, the three models agree on the contributions of the drivers to the TX anomaly (Fig. 7a). They estimate that recent climate change explains around 7 %–10 % of the event anomaly. CESM is the only model which shows a negative ocean contribution of around −7 %, whereas the role of the ocean is negligible in the other models. This result is supported by the studies by Dole et al. (2011) using initialized forecasts and Hauser et al. (2016) using an ESM, which both found a weak role of the ocean in explaining the Russian heatwave of 2010. In contrast, observation-based studies like Martius et al. (2012) and Trenberth and Fasullo (2012) linked the driving atmospheric circulation conditions to SST anomalies, identifying the ocean as an important driver. In all three models the event is mostly driven by atmospheric circulation and soil moisture, which agrees with existing literature. The ratio of the circulation contribution to the soil moisture contribution is 70 : 30 for EC-Earth and CESM and 80 : 20 for MIROC. Assessing the two approaches to disentangle atmospheric circulation from soil moisture contributions separately gives very similar results (Fig. A8a).

The European heatwave of 2015 consisted of four hot spells that were intensified by drought conditions through land–atmosphere feedbacks (Dong et al., 2016; Hauser et al., 2017a; Orth et al., 2016). The event is analyzed over the western and central Europe (WCE) AR6 reference region (Iturbide et al., 2020, see Fig. A3; same as central Europe – CEU – from previous assessment reports). The hottest 15 d period is from 2 to 16 August 2015 (Fig. 6b). The magnitude of the TX anomaly before and during the heatwave is represented well by all models. However, there are differences in the attribution of the drivers. In EC-Earth, climate change contributes around 12 % to the event anomaly, whereas in CESM climate change is estimated to contribute 22 % and in MIROC 34 % (Fig. 7b). EC-Earth and CESM agree that there is a small negative contribution by the ocean of −9 % and −7 %, respectively. In MIROC the ocean is negligible for the event anomaly (around −1 %). This is in contrast to the modeling study by Dong et al. (2016) and the observation-based study by Duchez et al. (2016), finding that the SST patterns set important preconditions for the 2015 European heatwave. The three ExtremeX models agree on the magnitude of the atmospheric circulation contribution, which is around half of the total event anomaly. However, the role of soil moisture depends on how much of the event anomaly is attributed to recent climate change. EC-Earth estimates the highest relative soil moisture contribution with a ratio of 60 : 40 between circulation and soil moisture. The ratio is 70 : 30 for CESM and 75 : 25 for MIROC. The results for the two disentangling approaches differ most notably for EC-Earth; the ratios are 65 : 35 for one approach (A) but nearly balanced for the other (B; Fig. A8b).

The US heatwave of 2012 evolved concurrently with a severe drought after an unusually warm winter and spring (Dole et al., 2014; Hoerling et al., 2014; H. Wang et al., 2014). The event is assessed for the region from 35 to 50° N and 55 to 110° W (see Fig. A3) and for 23 June to 7 July (Fig. 6c). The TX anomaly is represented well by MIROC and EC-Earth and a bit overestimated in CESM. The models agree well on the relative contribution of the drivers. In EC-Earth and CESM, recent climate change explains around 15 % of the event anomaly, whereas for MIROC it is slightly more (23 %, Fig. 7c). All models agree that the role of the ocean is very small, even if the sign is negative for EC-Earth and CESM (both −1 %) but positive for MIROC (6 %). This agrees with H. Wang et al. (2014) and Hoerling et al. (2014), who find the contribution by SSTs to be small. The three models agree that the role of soil moisture conditions is about equal to the role of atmospheric circulation. This is supported by earlier studies finding an important contribution by both the weather patterns and soil moisture deficit (Hoerling et al., 2014; PaiMazumder and Done, 2016; H. Wang et al., 2014). The ratio of circulation to soil moisture contribution is 50 : 50 for EC-Earth, 55 : 45 for CESM, and 60 : 40 for MIROC. The individual results for the disentangling approaches show that for all models soil moisture dominates for one approach (A), while atmospheric circulation dominates for the other (B; Fig. A8c).

At the time, the summer of 2012/13 was the warmest summer observed in Australia, but it has since then been surpassed by the 2018/19 and 2019/20 summers (Bureau of Meteorology, 2020). The Australian heatwave of 2012/13 is analyzed for the region from 18 to 30° S and 133 to 147° E (see Fig. A3). The hottest consecutive 15 d occur just at the beginning of 2013 from 1 to 15 January 2013 (Fig. 6d). The models represent the TX anomaly from ERA-Interim mostly well, except that in MIROC it is underestimated during the first half of the event period. While the contribution by recent climate change to the event anomaly is very small and negative in EC-Earth (−2 %), CESM and MIROC agree on a small but positive contribution (7 % and 10 %, respectively, Fig. 7d). All models show a negative contribution of the ocean, which is most notable in CESM (around −25 %), while in EC-Earth it is smaller (−7 %) and almost negligible in MIROC (−2 %). This is in line with the La Niña conditions that prevailed from mid-2010 to early 2012 and then remained neutral for the rest of 2012 and during 2013 (NOAA Climate Prediction Center, 2022) as well as with the findings by Lewis and Karoly (2013). For EC-Earth and CESM the contribution by the atmospheric circulation is larger than by soil moisture, whereas for MIROC it is the other way around. It was also found by King et al. (2014) that the dry conditions were an important driver of the heatwave. The ratio of atmospheric circulation contribution to soil moisture contribution is 60 : 40 for EC-Earth, 55 : 45 for CESM, and 40 : 60 for MIROC. For MIROC, the individual ratios from the two disentangling approaches both agree that the contribution of soil

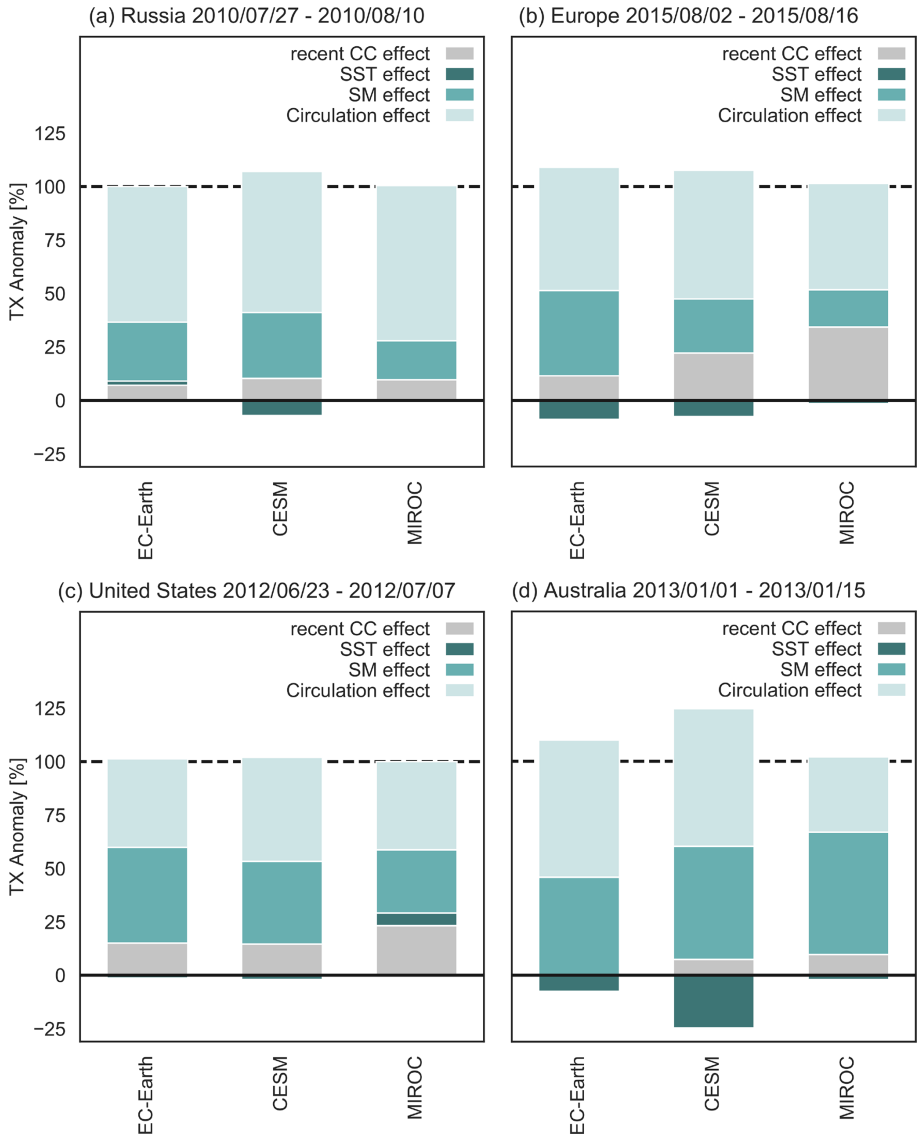

Figure 7. Contribution of recent climate change (since the 1982–2008 base period) and physical drivers to the daily maximum temperature (TX) anomaly during 4 recent events: **(a)** Russia 2010, **(b)** Europe 2015, **(c)** United States 2012, **(d)** Australian summer 2012/13. The dates of the hottest consecutive 15 d period are given in the label of each subplot. The contributions of the drivers are normalized by the climatology of AF_SF for each model. The two approaches to compute SM vs. ATM contribution are merged, giving equal weight to both.

moisture is larger than the contribution of the atmospheric circulation to the event anomaly, whereas for the other two models the individual ratios reflect the fact that the contribution by the two main drivers of the Australian heatwave is equal to slightly circulation-dominated according to the experiments (Fig. A8d). This may reflect the fact that the warm bias simulated by MIROC is significantly alleviated with the soil moisture constrained experiment (Fig. 4).

Overall, the three models mostly agree on the relative contribution of atmospheric circulation vs. soil moisture to the TX anomaly during four recent heatwaves. For the heatwaves of 2010 in Russia and 2015 in Europe, all models show that the atmospheric circulation plays the most important role. For the US heatwave of 2012, the models agree that soil moisture conditions are about as important as atmospheric circulation for driving the TX anomaly. For the Australian heatwave of 2012/13, two models show that atmospheric circulation is more important, whereas one model shows that the soil moisture contribution was largest. All models agree on a small role of climate change in driving the TX anomaly during the 2010 Russian heatwave and the 2012/13 heatwave in Australia. However, for the 2015 European heatwave and the US heatwave in 2012, the role of climate change differs between the models, being largest for MIROC and smallest for EC-Earth. The role of the ocean is small for the heatwaves of 2010 in Russia, 2015 in Europe, and 2012 in the US. For

the 2012/13 heatwave in Australia, all models agree that the role of the ocean is negative, thus not enhancing the heatwave; however, the models disagree on the magnitude, with CESM being the only model displaying a notable contribution by the ocean.

5.2 Relative contribution of atmospheric circulation and soil moisture to episodes of anomalously warm temperatures

In the following, we analyze the role of atmospheric circulation and soil moisture in driving the occurrence of warm spells during 1982–2015/16 (2015 for MIROC and 2016 for the other two models). The disentangling method is the same as used previously in Sect. 5.1. Warm spells are defined grid-point-wise as time periods during the local summer season when daily mean temperature anomalies in ERA-Interim exceed 1.5 SD (standard deviation) of the 1982–2010 climatology for at least 3 consecutive days. A 7 d running mean is applied to the years 1982–2010 from ERA-Interim before computing the daily climatology and standard deviation. The local summer season is defined as the hottest consecutive 3 months (from ERA-Interim) for each grid point. The threshold of 1.5 SD was chosen such that most regions of the world actually experience events. However, using 1 or 2 SD as the threshold leads to very similar results (not shown). The identified warm spells are categorized into events of 3–5 d, 6–13 d, and 14 d or longer. The choice of categories was made to separate events lasting a few days from week-long events and very long-lasting events of 2 weeks or more. Also, the choice was made to obtain a reasonable sampling size for each category. The warm spells based on ERA-Interim are analyzed by taking the same dates (calendar year and days of the year) in the experiments. First, the same dates are analyzed for the fully constrained (AF_SF) experiment to determine the model truth for each event and model (using the ensemble mean for MIROC, which has five simulation runs). Then, the contribution of the drivers is disentangled according to Fig. 2. One or five simulation runs (over the years 1982–2015/16) are used, depending on how many were available per model and experiment. The mean temperature anomaly of each event category and experiment (averaged over all events and simulation runs) is used to disentangle the relative contribution of the atmospheric circulation and soil moisture conditions grid-point-wise.

The agreement among models is very high for all spell lengths (Fig. 8). The grid points for which soil moisture contributes one-third or more to the warm spells agree well with the regions of high soil moisture–temperature coupling (Koster et al., 2004; Miralles et al., 2012). With increasing spell length, the contribution of soil moisture becomes more important, for example in the US Midwest, Eurasia, and northern Australia. Further, with a longer spell length there is a growing proportion of total soil moisture contribution, as can be seen by the increasing percentage of soil moisture dominance for all models in Fig. 8. This shows the growing relative importance of the land surface–atmosphere coupling for long-duration events.

The analysis also reveals that warm spells of 14 d or longer with a magnitude of more than 1.5 SD do not occur often or in many regions of the world. The result for eastern Europe, for example, can be traced back to the Russian heatwave in 2010. For tropical regions like Amazonia or very dry regions like the Sahara, it is not always possible to disentangle the relative contributions of atmosphere and soil moisture. This occurs because the computed differences can become negative if the less constrained experiments have a higher temperature anomaly than the more constrained experiments on average. The affected grid cells are masked out in white in Fig. 8.

It has to be noted that the analysis method takes into account the temporal persistence of warm spells but not temporal correlation such as the time-lagged effect of dry springs on hot summers (e.g., Hirschi et al., 2011; Quesada et al., 2012). Furthermore, the events are only identified grid-point-wise and not as spatially coherent patterns, as they would occur naturally. This is responsible for some of the noise in the patterns.

6 Conclusions and outlook

The ExtremeX experiment is a multi-model intercomparison project designed to study processes contributing to the occurrence and intensity of extreme events. ExtremeX currently consists of simulations with three ESMs: EC-Earth3, MIROC5, and CESM1.2. Five experiments were run with all models, with one or more of the models' components being constrained. SSTs and sea ice coverage fractions are prescribed in all experiments. A grid-point nudging approach is used to constrain the modeled horizontal winds in the atmosphere, and soil moisture prescription is used to constrain the land surface.

Although the constrained experiments capture the temporal evolution and magnitude of temperature anomalies well during recent heatwave events, climatological biases in temperature and precipitation remain in the experiments. This is the case for experiments with either nudged atmospheric circulation patterns and/or prescribed soil moisture conditions. In some cases, biases are enhanced or even change sign in the constrained experiments (Figs. 3–5). Comparing the location and magnitude of the climatological biases reveals that the patterns and sign of the biases often remain and the magnitude is only marginally reduced. This agrees with findings by Wehrli et al. (2018) for atmospheric nudging in CESM. The results suggest that the biases are caused by other processes such as cloud and precipitation formation, convection, interactions of the land surface and the ocean with the atmosphere, or also land surface parameters. It is also likely that none of these other elements is the sole explanation for the

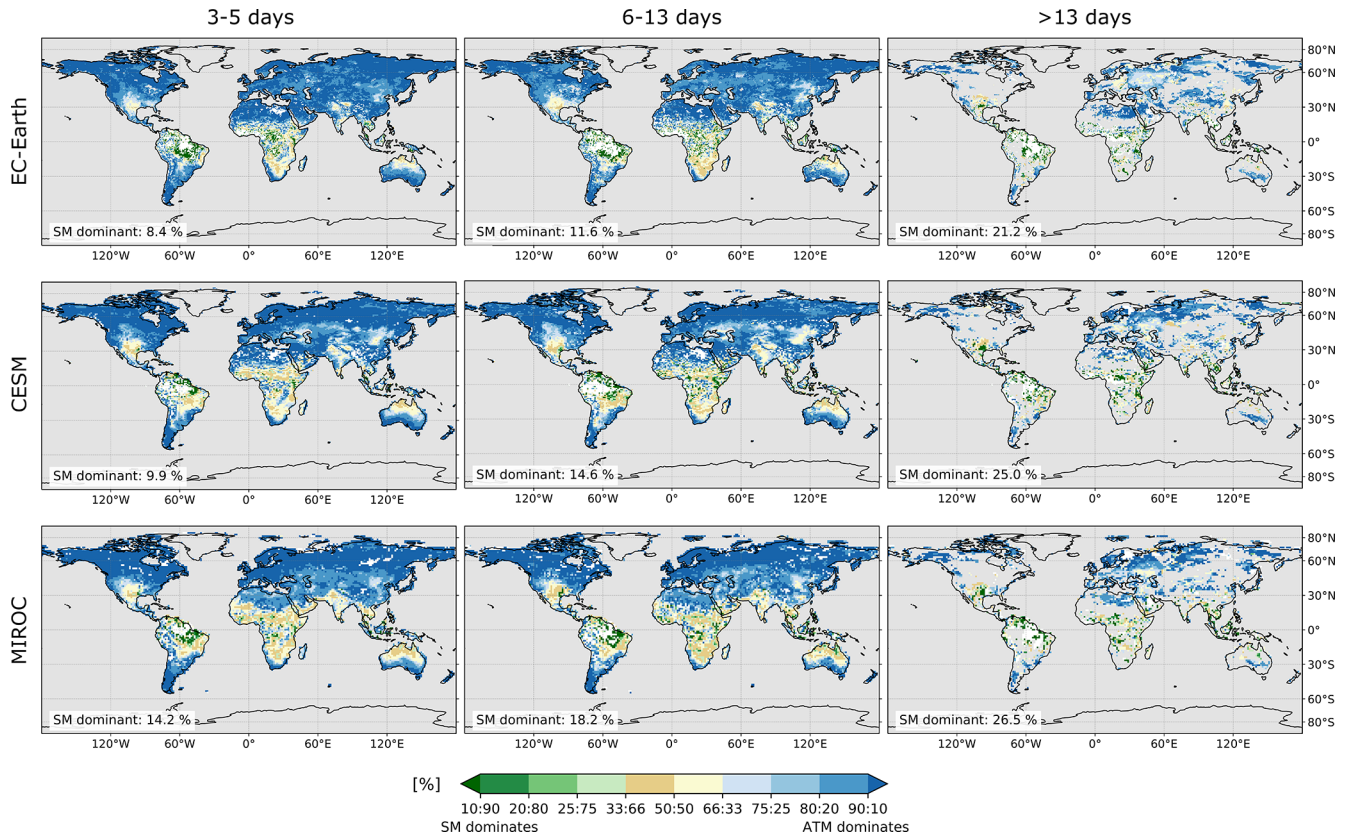

Figure 8. Contribution of atmospheric circulation (ATM) vs. soil moisture (SM) to warm spells during the local summer season when daily mean temperature anomalies exceed 1.5 SD (standard deviation) from the ERA-Interim 1981–2010 climatology. The local summer season is defined as the hottest consecutive 3 months (from ERA-Interim) for each grid point. The two approaches to compute the SM vs. ATM contribution are merged, giving equal weight to both. Events are categorized into spells lasting 3–5 d, 6–13 d, and 14 d or longer. Ocean grid points, Antarctica, Greenland, and Iceland are masked out in grey using the Greenland–Iceland (GIC) region from the AR6 reference regions for the latter two. Grid points for which no events were identified are also masked out in grey. Grid points for which the contributions could not be determined (see text) are masked out in white. In the lower left corner the grid points for which the SM contribution dominates over the ATM contribution ($> 50\,\%$) are given as an area-weighted percentage with respect to all valid grid points.

climatological biases, but rather their interaction, including atmospheric circulation and soil moisture (dynamics) interactions.

Despite the biases in mean climatology, the experiments with constrained atmosphere and soil moisture can accurately reproduce temperature anomalies during and prior to heatwaves (Fig. 6). This is found for all models and supports the results by Wehrli et al. (2019) for CESM. This result implies that bias correction could alternatively be used to improve the representation of extreme events in the models instead of analyzing anomalies as is done here. The presented set of experiments can be used for extreme event analysis as long as the atmospheric circulation and/or soil moisture are major drivers of the event. The experiments are not ideal if the focus is on the role of the ocean because the ocean is prescribed. For events that are mainly ocean-driven, we would recommend a setup with interactive ocean experiments to compute the ocean contribution more accurately. This would apply, for example, to extreme events (i.e., droughts, heatwaves, floods) that are strongly driven by the El Niño–Southern Oscillation and other coupled ocean–atmosphere phenomena such as the Indian Ocean Dipole or the Pacific Decadal Oscillation. Nevertheless, here we derive the potential ocean contribution by comparing the anomaly to non-event years. The present study disentangles the role of atmospheric circulation vs. land surface processes for temperature anomalies. Therefore, additivity of the different contributions is assumed. This is inspired by the study by Kröner et al. (2017) for summer climate in Europe. Following the disentangling in Wehrli et al. (2019), experiments with constrained soil moisture (AI_SF) and with a nudged atmosphere and soil moisture constrained to climatological values (AF_SC) are used along with the control (AI_SI) and fully constrained (AF_SF) experiments. The experiment with a nudged atmosphere and interactive soil moisture (AF_SI) leads to similar temperature anomalies during heatwaves like the AF_SF experiment. Atmospheric nudging strongly constrains land surface conditions due to the control on available

moisture, and because in AF_SF ERA-Interim is used to derive the target soil moisture that is prescribed, similar land surface conditions result in both experiments. Hence, AF_SI is not considered in the disentangling procedure (see Fig. 2). To have more robust results, two disentangling approaches are considered like in Wehrli et al. (2019). Both approaches tend to produce similar results, indicating that in a first-order assumption the contributions can be treated as additive. Nevertheless, it has to be noted that disentangling causality in a coupled system always comes with limitations. Differences between the approaches show nonlinearities in the responses due to feedbacks.

TX anomalies during four recent heatwaves are attributed to their physical drivers and to climate change. The four events considered are the 2010 Russian heatwave, the 2012 heatwave in the US, the Australian heatwave of 2012/13, and the European heatwave in 2015. Overall the models show good agreement on the role of the drivers. Recent warming (since 1982–2008) is found to positively contribute to the event anomaly for all events and nearly all models (not for the Australian heatwave of 2012/13 and EC-Earth). The largest contribution by recent warming is found for the US heatwave of 2012 (15 %–23 %) and for the European heatwave of 2015. However, for the latter event the three models agree less on the relative role of climate change (12 %–34 %). In the presented setup the ocean was not found to have a substantial role in driving any of the events considered. This could be due to the limited interaction between the ocean and the atmosphere due to the prescription of SSTs and sea ice or because the ocean was indeed not a driver of the events considered. For the Australian heatwave of 2012/13, the ocean is found to influence the temperature anomaly negatively in CESM (−23 %). This is in accordance with the cool to neutral phase of the El Niño–Southern Oscillation (NOAA Climate Prediction Center, 2022). For all four heatwaves the models show that both atmospheric circulation and land surface conditions significantly contribute to the event anomaly. For the Russian heatwave of 2010 and the European heatwave of 2015, atmospheric circulation is the dominant driver, with land surface conditions playing a secondary but still important role. Yet, for the US heatwave 2012, soil moisture is about as important as atmospheric circulation. For the Australian heatwave of 2012/13, one model shows that soil moisture is the most important driving factor, and the other two models show that the two physical drivers are about equally important. Note that, by design, the ExtremeX framework does not give information on which of the drivers is the initial source of the heatwaves since the constraining of the model components was carried out for the whole simulation period and events were analyzed using contemporaneous anomalies from the experiments.

The ExtremeX experiments also allow a general assessment of the respective contributions of circulation anomalies vs. soil moisture conditions for warm spells. The results are very similar for the three ESMs, showing that the models generally agree on the representation of extreme events and the driving processes behind these events. Warm spells of at least 3 d are assessed grid-point-wise and show that soil moisture is responsible for around one-third to half of the temperature anomalies in transitional and tropical climate zones (Fig. 8). The regions identified resemble the regions of strong soil moisture–temperature coupling highlighted by Miralles et al. (2012) for observational data and Seneviratne et al. (2006) for global climate models. Both studies additionally identify southern Europe and Eurasia as regions of strong soil moisture–temperature coupling, which is, however, not confirmed by the results presented here. Nevertheless, in regions where spells of at least 2 weeks can occur – like in Eurasia – soil moisture is more important for these longer events than for shorter events, driving up to one-third of the temperature anomaly.

This study expands the mechanistic analysis of recent heatwaves by Wehrli et al. (2019) using three Earth system models. The results for warm spells at the grid-point level and for the four heatwaves suggest that both circulation patterns and soil moisture anomalies substantially contribute to the occurrence of heat extremes, which is consistent with Wehrli et al. (2019). Soil moisture effects are particularly important in the tropics, monsoon regions, and the US Great Plains, while circulation anomalies tend to dominate in other regions of the extratropics. These results can help to shed light on processes that need to be better taken into account in weather predictions and climate projections. For instance, the important role of soil moisture conditions for extremes suggests that soil moisture monitoring and initialization could substantially improve forecasting of weather extremes in several regions.

Appendix A

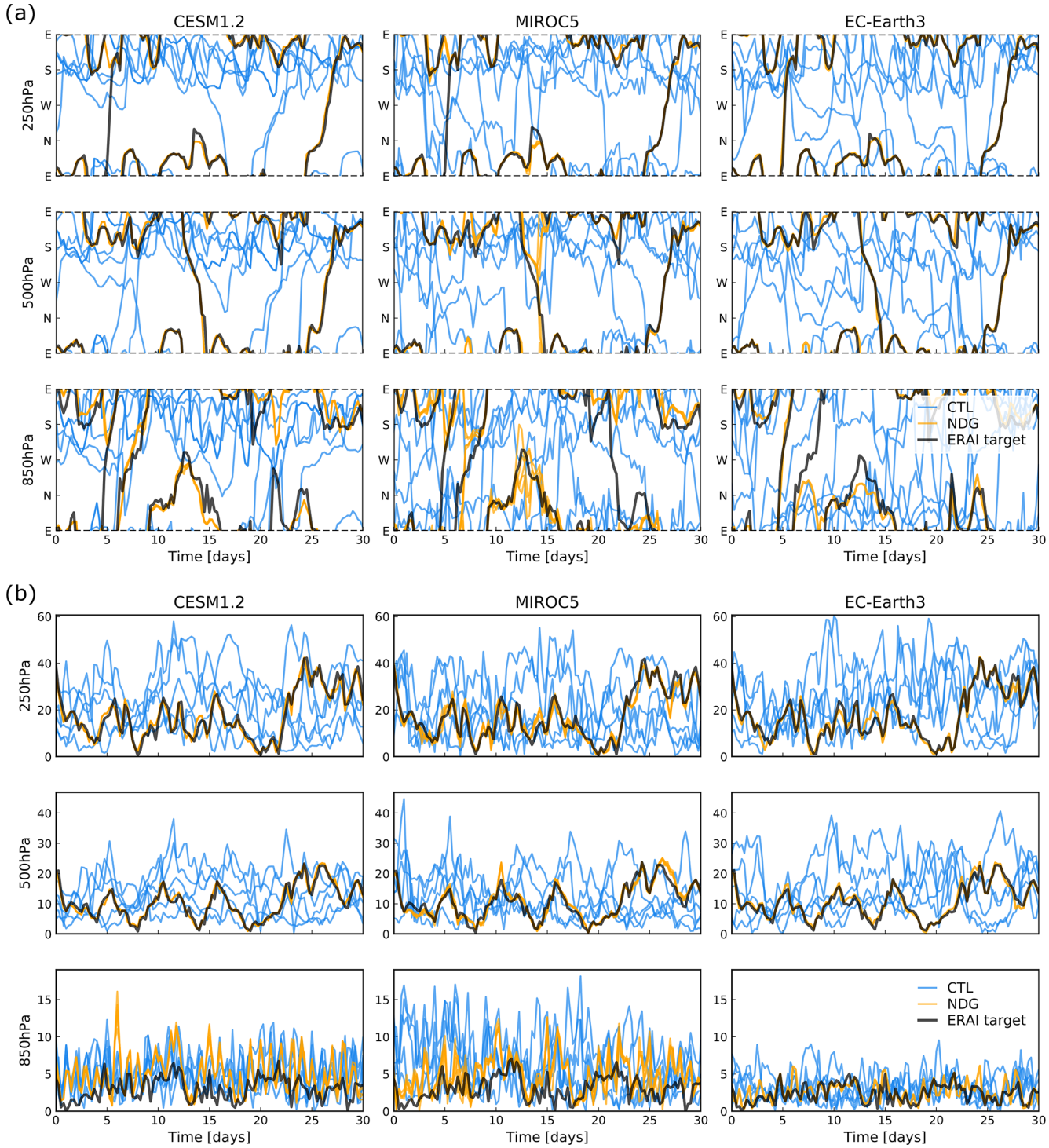

Figure A1. Comparison of winds for the experiments with a nudged atmosphere (NDG, corresponds to AF_SI) and free atmosphere (CTL, corresponds to AI_SI). Shown are 6-hourly wind direction **(a)** and wind speed **(b)** during 1 month (June 2000) for one grid point over the Alps. The winds from the models were interpolated to 250, 500, and 850 hPa. The winds from ERA-Interim (ERAI target) were interpolated to the same pressure levels and the model resolution for each model.

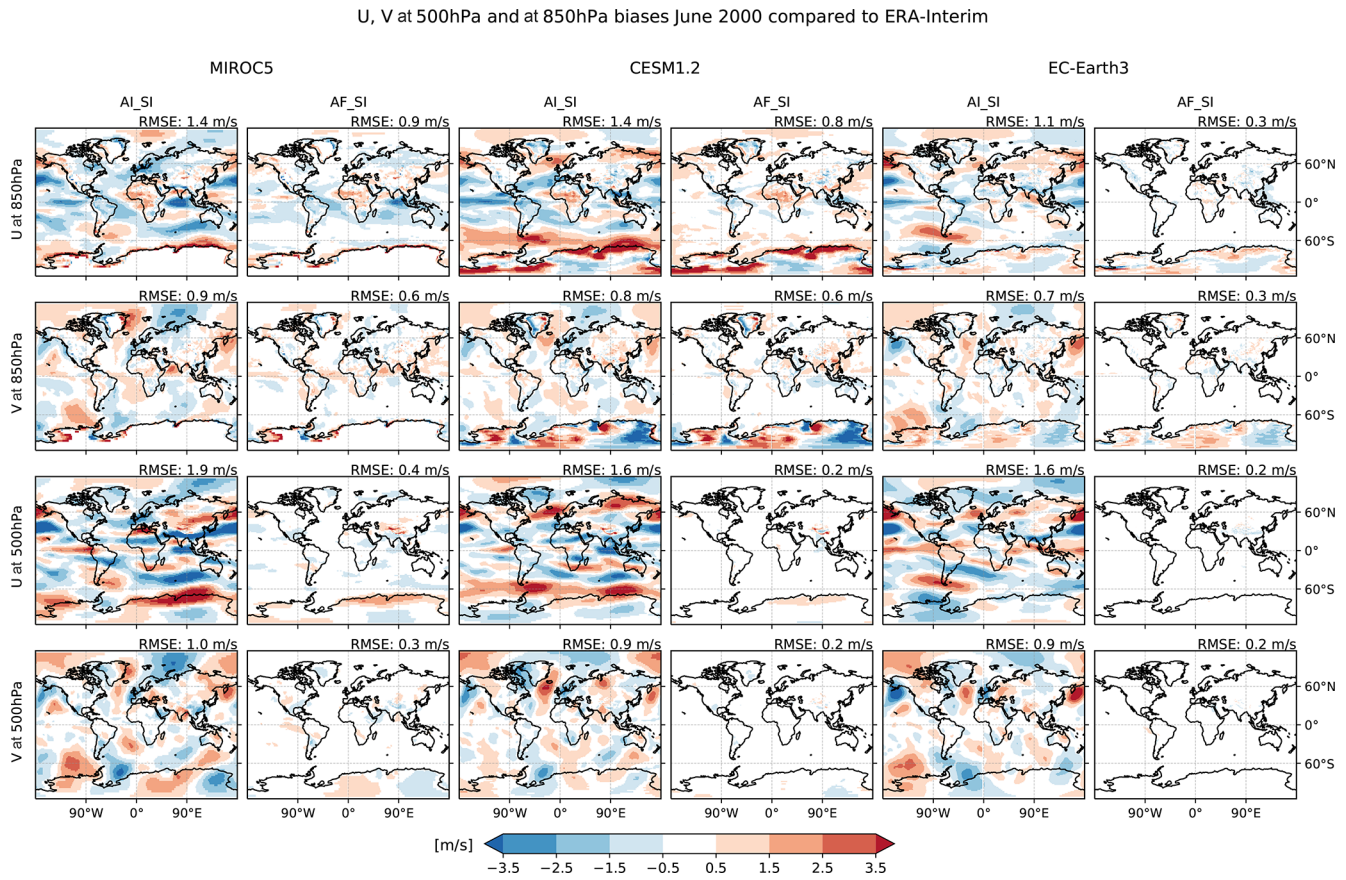

Figure A2. Bias of the zonal (U) and meridional (V) wind components at 850 and 500 hPa for the experiments with a nudged atmosphere (AF_SI) and free atmosphere (AI_SI), showing the ensemble mean when multiple simulations are available. Shown is the average of 6-hourly wind fields for 1 month (June 2000). The winds from the models were interpolated to 500 and 850 hPa. The winds from ERA-Interim were interpolated to the same pressure levels and the model resolution for each model.

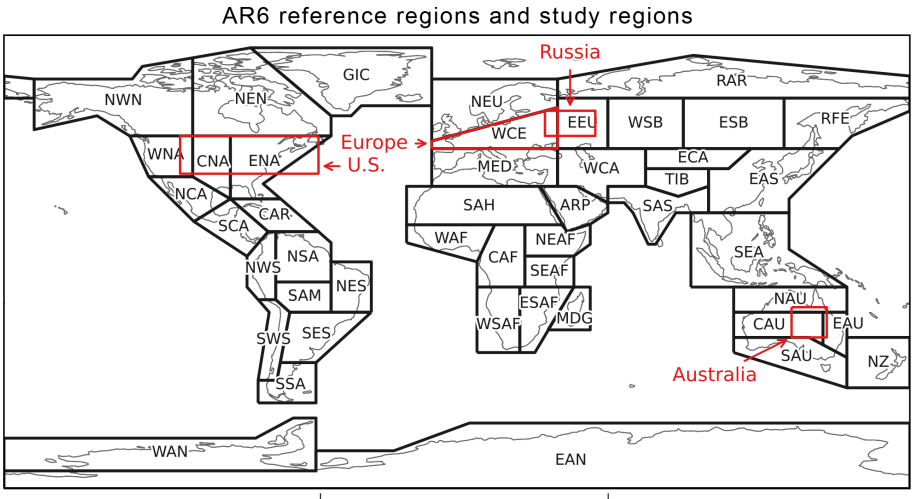

Abbrev.	Name	Abbrev.	Name	Abbrev.	Name
GIC	Greenland/Iceland	NEU	N.Europe	RFE	Russian-Far-East
NWN	N.W.North-America	WCE	West&Central-Europe	WCA	W.C.Asia
NEN	N.E.North-America	EEU	E.Europe	ECA	E.C.Asia
WNA	W.North-America	MED	Mediterranean	TIB	Tibetan-Plateau
CNA	C.North-America	SAH	Sahara	EAS	E.Asia
ENA	E.North-America	WAF	Western-Africa	ARP	Arabian-Peninsula
NCA	N.Central-America	CAF	Central-Africa	SAS	S.Asia
SCA	S.Central-America	NEAF	N.Eastern-Africa	SEA	S.E.Asia
CAR	Caribbean	SEAF	S.Eastern-Africa	NAU	N.Australia
NWS	N.W.South-America	WSAF	W.Southern-Africa	CAU	C.Australia
NSA	N.South-America	ESAF	E.Southern-Africa	EAU	E.Australia
NES	N.E.South-America	MDG	Madagascar	SAU	S.Australia
SAM	South-American-Monsoon	RAR	Russian-Arctic	NZ	New-Zealand
SWS	S.W.South-America	WSB	W.Siberia	EAN	E.Antarctica
SES	S.E.South-America	ESB	E.Siberia	WAN	W.Antarctica
SSA	S.South-America				

Figure A3. Reference regions of the IPCC AR6 as defined in Iturbide et al. (2020). The event regions used in Sect. 5.1 are indicated in red.

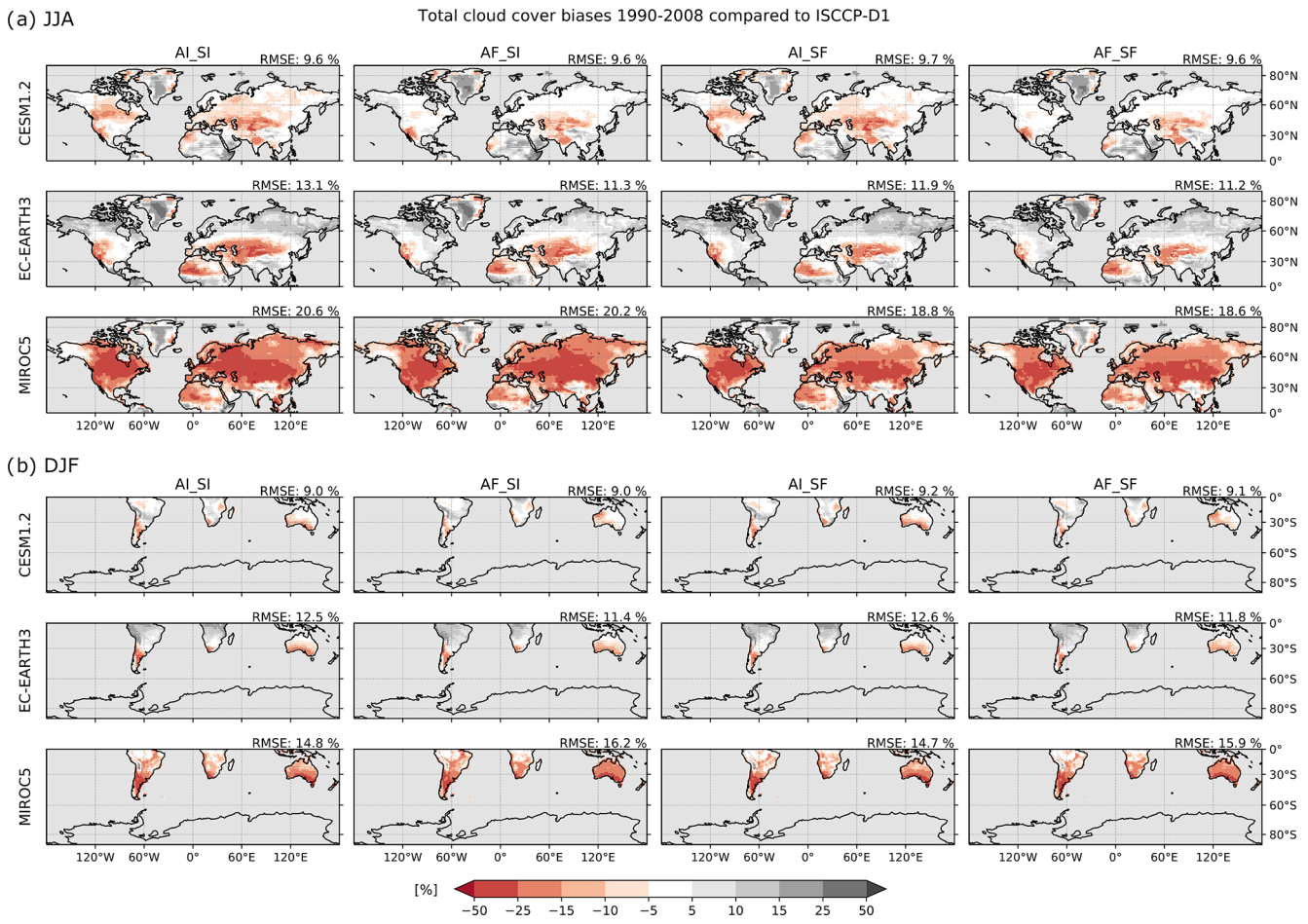

Figure A4. Bias in total cloud cover with respect to ISCCP-D1. Average over **(a)** JJA for the Northern Hemisphere and **(b)** DJF for the Southern Hemisphere. Ocean grid points and Antarctica are masked out. The RMSE averaged over all valid grid points of the respective hemisphere is given in millimeters per day in the upper right corner of each experiment and model.

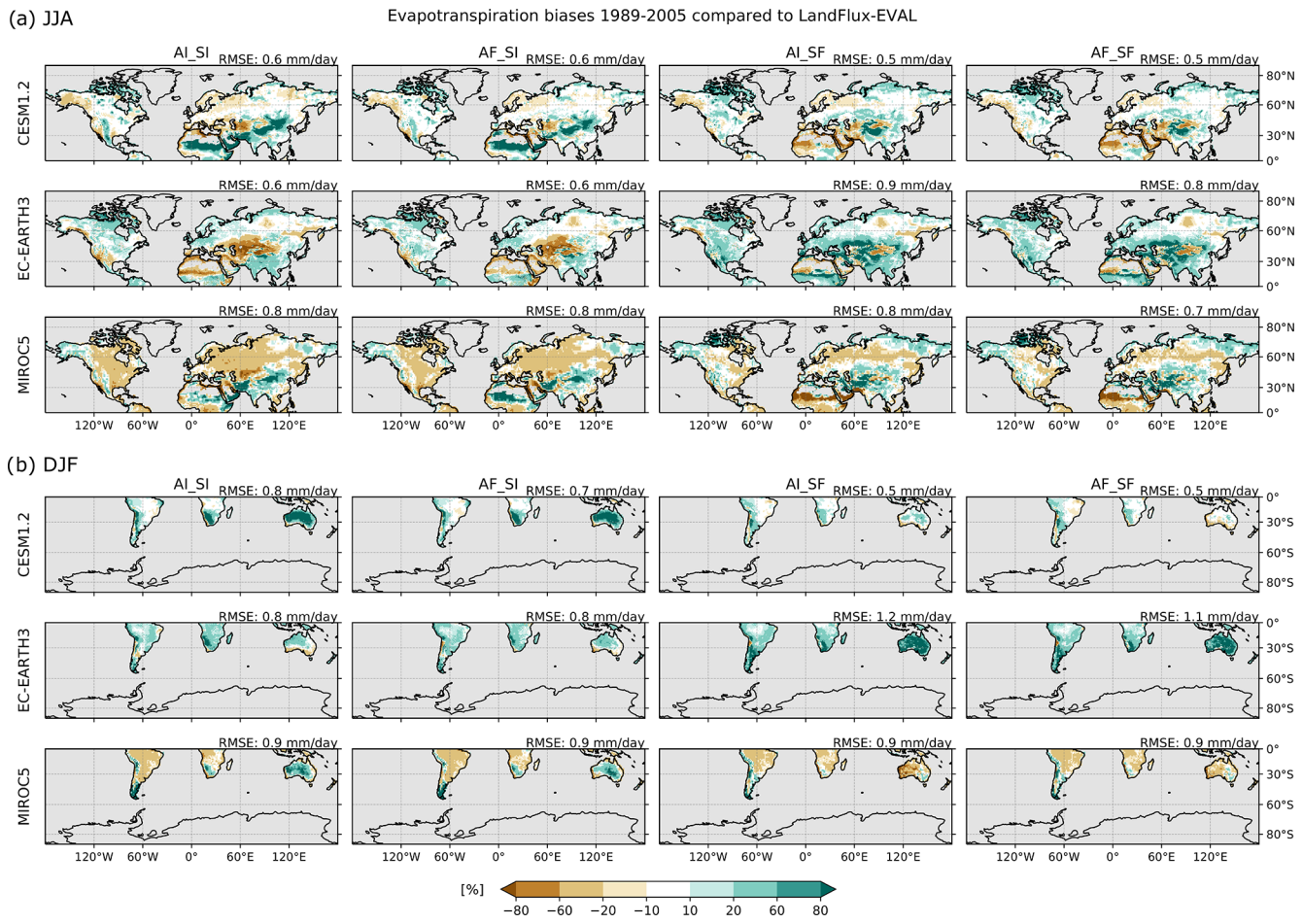

Figure A5. Bias in evapotranspiration with respect to LandFlux-Eval. Average over **(a)** JJA for the Northern Hemisphere and **(b)** DJF for the Southern Hemisphere. Masked out are grid points with a seasonal average of less than 0.1 mm evapotranspiration per day in the reference data set. Additionally, ocean grid points, grid points north of 75° N, Antarctica, Greenland, and Iceland are masked out using the Greenland–Iceland (GIC) region from the AR6 reference regions for the latter two. The RMSE averaged over all valid grid points of the respective hemisphere is given in millimeters per day in the upper right corner of each experiment and model.

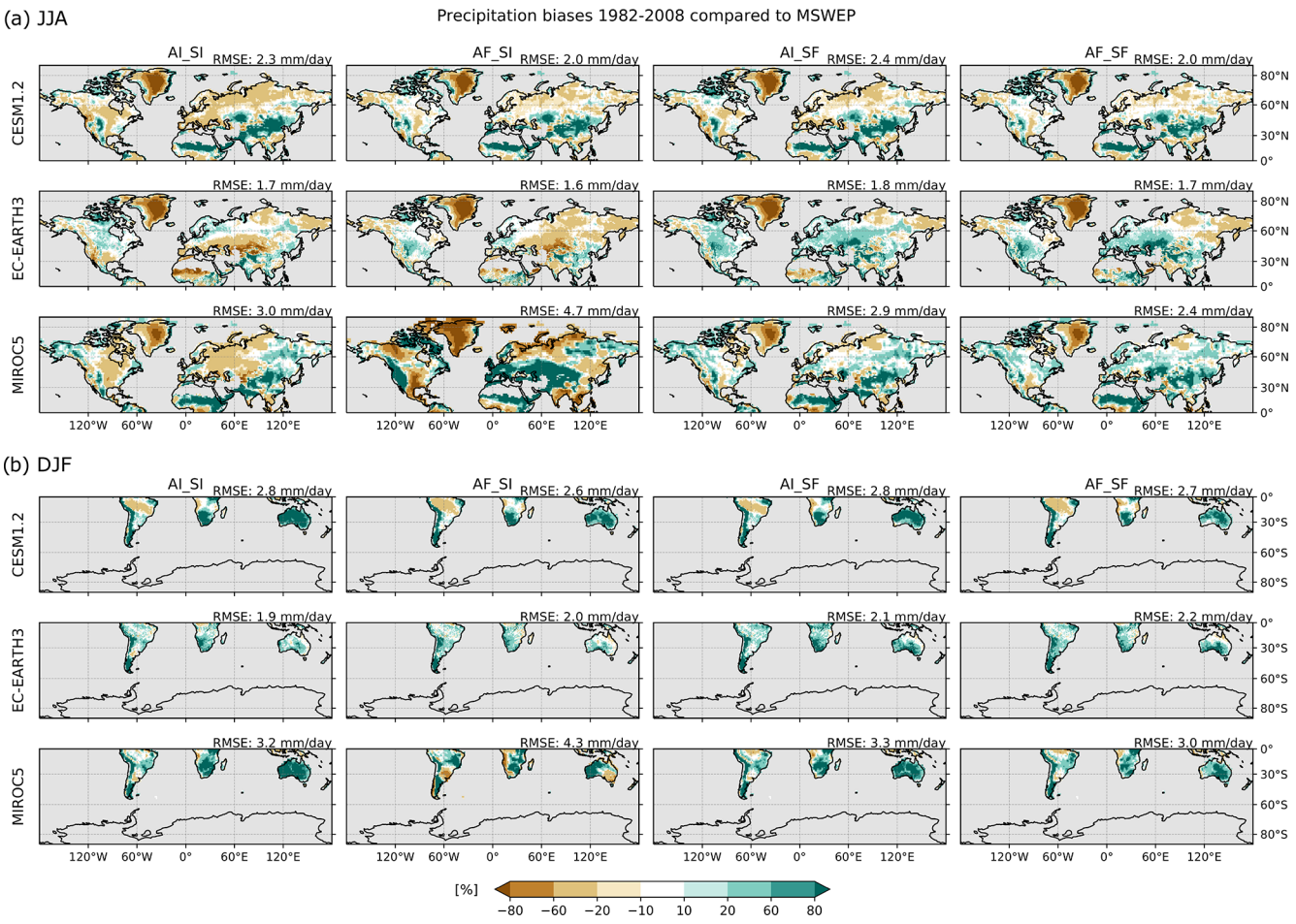

Figure A6. Same as Fig. 5 but using MSWEP as a reference data set.

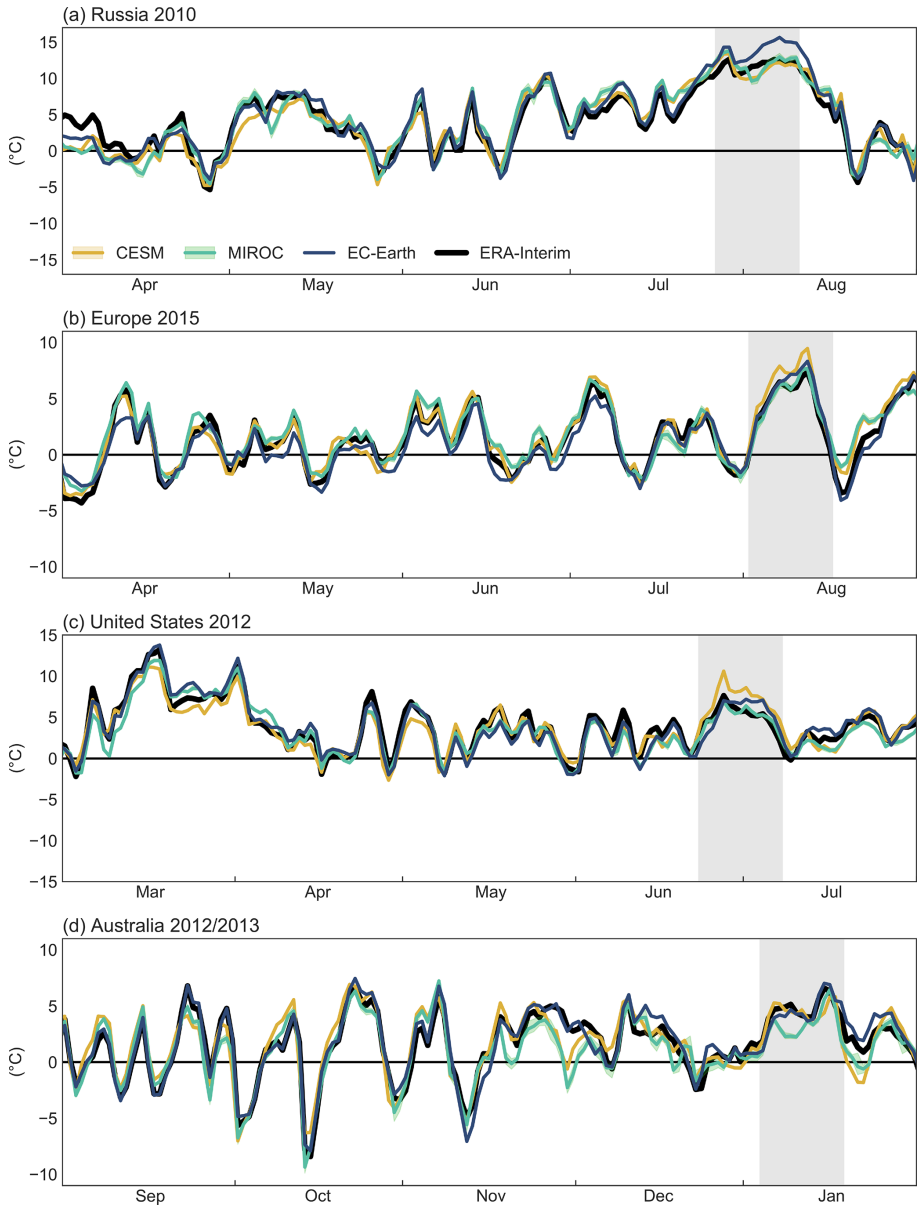

Figure A7. Same as Fig. 6 but for the nudging experiment (AF_SI). The shading shows the full ensemble spread and lines the ensemble mean (or single simulation for EC-Earth).

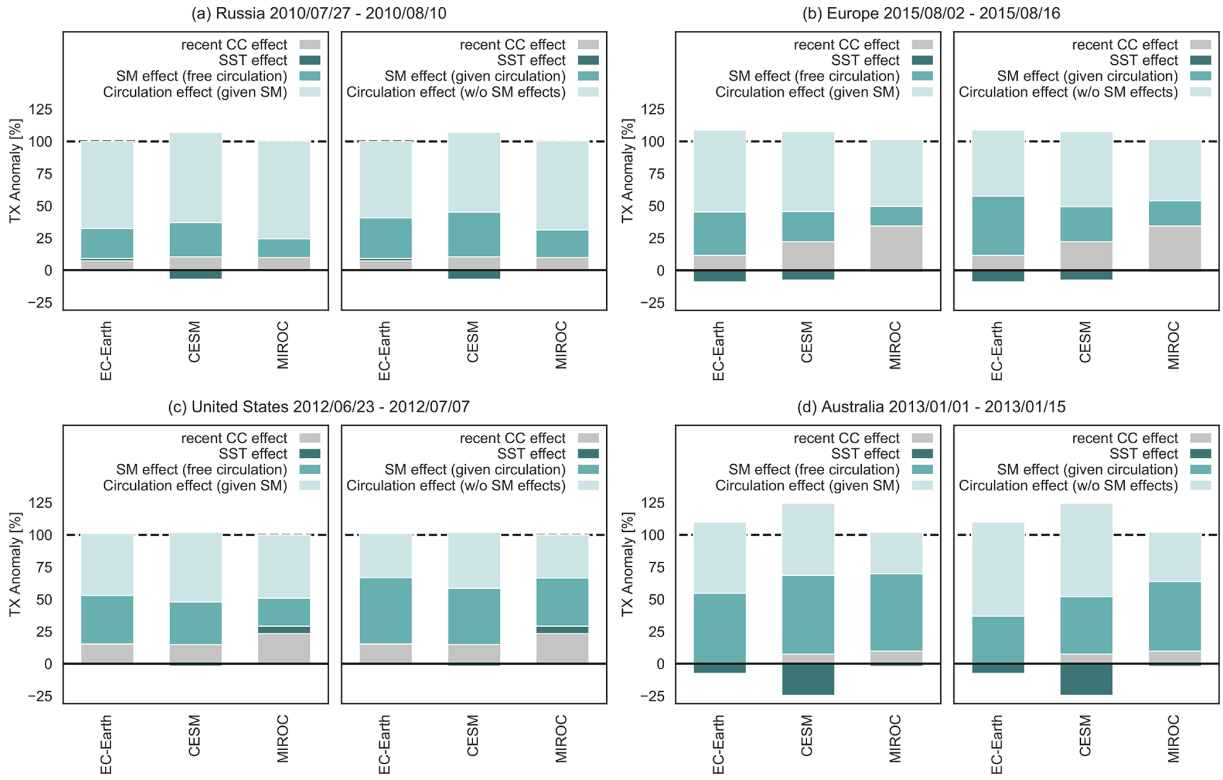

Figure A8. Same as Fig. 7 but showing the separate effects for the two approaches to compute SM vs. ATM contributions (left A, right B).

Code availability. The analysis code can be made available by the authors upon request.

Data availability. Simulation data from the models are available from https://data.iac.ethz.ch/Wehrli_et_al_2022_ExtremeX/ (Wehrli et al., 2022).

Author contributions. KW, MH, and SIS designed the experiments with input from OM and RV. FL ran the EC-Earth3 simulations with technical help from FS, WM, and PLS. HS ran the interactive and atmosphere nudged simulations with MIROC5. DT and HK ran the soil moisture nudged simulations with MIROC5. KW ran the CESM1.2 model simulations with technical support by MH. KW analyzed the results from all models. KW, FL, MH, HS, DT, HK, DC, WM, OM, RV, and SIS contributed to the discussion of results. KW prepared the paper with contributions from all co-authors.

Competing interests. The contact author has declared that none of the authors has any competing interests.

Disclaimer. Publisher's note: Copernicus Publications remains neutral with regard to jurisdictional claims in published maps and institutional affiliations.

Acknowledgements. MIROC5 simulations were contributed by NIES Japan and the University of Tokyo. EC-Earth3 simulations were contributed by VU Amsterdam and KNMI. CESM1.2 simulations were contributed by ETH Zurich. The authors thank the editor, Paul Dirmeyer, and one anonymous reviewer for their valuable comments and suggestions on the paper. The authors also thank Dominik Schumacher for his feedback on the revised paper. Kathrin Wehrli and Sonia I. Seneviratne acknowledge funding from the European Research Council (ERC) (DROUGHT-HEAT project, grant 617518). Fei Luo, Dim Coumou, and Frank Selten acknowledge a VIDI award from the Netherlands Organisation for Scientific Research (NWO) (Persistent Summer Extremes "PERSIST" project). Hideo Shiogama was supported by the Integrated Research Program for Advancing Climate Models (JPMXD0717935457). Hyungjun Kim acknowledges the National Research Foundation of Korea (NRF) grant funded by the Korean Government (MSIT) (2021H1D3A2A03097768 and NRF-2018R1A5A7025409). Wilhelm May is supported through the Swedish strategic research area ModElling the Regional and Global Earth system (MERGE). The MIROC5 simulations were performed using the Earth Simulator in JAMSTEC and the NEC SX in NIES. The authors acknowledge the support of Matthieu Leclair and Benoit P. Guillod in the design of the experiments and advice during the course of

the project. This study uses the LandFlux-EVAL merged benchmark synthesis products of ETH Zurich produced under the aegis of the GEWEX and ILEAPS projects (http://www.iac.ethz.ch/url/research/LandFlux-EVAL/, last access: 26 July 2022).

Financial support. This research has been supported by the European Research Council under FP7 Ideas: European Research Council (DROUGHT-HEAT (grant no. 617518)), the Nederlandse Organisatie voor Wetenschappelijk Onderzoek (grant no. 016.Vidi.171011), the Japan Ministry of Education, Culture, Sports, Science and Technology (grant no. JPMXD0717935457), and the National Research Foundation of Korea (NRF) grant funded by the Korean Government (MSIT) (2021H1D3A2A03097768 and NRF-2018R1A5A7025409).

Review statement. This paper was edited by Laurens Ganzeveld and reviewed by Paul Dirmeyer and one anonymous referee.

References

Angélil, O., Perkins-Kirkpatrick, S., Alexander, L. V., Stone, D., Donat, M. G., Wehner, M., Shiogama, H., Ciavarella, A., and Christidis, N.: Comparing regional precipitation and temperature extremes in climate model and reanalysis products, Weather Clim. Extrem., 13, 35–43, https://doi.org/10.1016/j.wace.2016.07.001, 2016.

Arblaster, J. M., Lim, E.-P., Hendon, H. H., Trewin, B. C., Wheeler, M. C., Liu, G., and Braganza, K.: Understanding Australia's hottest September on record, B. A. Meteorol. Soc., 95, 37–41, https://doi.org/10.1175/1520-0477-95.9.S1.1, 2014.

Balsamo, G., Beljaars, A., Scipal, K., Viterbo, P., van den Hurk, B., Hirschi, M., and Betts, A. K.: A revised hydrology for the ECMWF model: verification from field site to terrestrial water storage and impact in the integrated forecast system, J. Hydrometeorol., 10, 623–643, https://doi.org/10.1175/2008JHM1068.1, 2009.

Balsamo, G., Albergel, C., Beljaars, A., Boussetta, S., Brun, E., Cloke, H., Dee, D., Dutra, E., Muñoz Sabater, J., Pappenberger, F., de Rosnay, P., Stockdale, T., and Vitart, F.: ERA-Interim/Land: a global land surface reanalysis data set, Hydrol. Earth Syst. Sci., 19, 389–407, https://doi.org/10.5194/hess-19-389-2015, 2015.

Barriopedro, D., Fischer, E. M., Luterbacher, J., Trigo, R. M., and García-Herrera, R.: The hot summer of 2010: Redrawing the temperature record map of Europe, Science, 332, 220–224, https://doi.org/10.1126/science.1201224, 2011.

Beck, H. E., Wood, E. F., Pan, M., Fisher, C. K., Miralles, D. G., van Dijk, A. I. J. M., McVicar, T. R., and Adler, R. F.: MSWEP V2 global 3-hourly 0.1° precipitation: methodology and quantitative assessment, B. Am. Meteorol. Soc., 100, 473–500, https://doi.org/10.1175/BAMS-D-17-0138.1, 2018.

Bony, S., Stevens, B., Frierson, D. M. W., Jakob, C., Kageyama, M., Pincus, R., Shepherd, T. G., Sherwood, S. C., Siebesma, A. P., Sobel, A. H., Watanabe, M., and Webb, M. J.: Clouds, circulation and climate sensitivity, Nat. Geosci., 8, 261–268, https://doi.org/10.1038/ngeo2398, 2015.

Brands, S.: A circulation-based performance atlas of the CMIP5 and 6 models for regional climate studies in the Northern Hemisphere mid-to-high latitudes, Geosci. Model Dev., 15, 1375–1411, https://doi.org/10.5194/gmd-15-1375-2022, 2022.

Brunner, L., Pendergrass, A. G., Lehner, F., Merrifield, A. L., Lorenz, R., and Knutti, R.: Reduced global warming from CMIP6 projections when weighting models by performance and independence, Earth Syst. Dynam., 11, 995–1012, https://doi.org/10.5194/esd-11-995-2020, 2020.

Bureau of Meteorology: Extreme heat and fire weather in December 2019 and January 2020, Spec. Clim. Statement, 73http://www.bom.gov.au/climate/current/statements/scs73.pdf (last access: 26 July 2022), 2020.

Dee, D. P., Uppala, S. M., Simmons, A. J., Berrisford, P., Poli, P., Kobayashi, S., Andrae, U., Balmaseda, M. A., Balsamo, G., Bauer, P., Bechtold, P., Beljaars, A. C. M., van de Berg, L., Bidlot, J., Bormann, N., Delsol, C., Dragani, R., Fuentes, M., Geer, A. J., Haimberger, L., Healy, S. B., Hersbach, H., Hólm, E. V., Isaksen, L., Kållberg, P., Köhler, M., Matricardi, M., McNally, A. P., Monge-Sanz, B. M., Morcrette, J.-J., Park, B.-K., Peubey, C., de Rosnay, P., Tavolato, C., Thépaut, J.-N., and Vitart, F.: The ERA-Interim reanalysis: configuration and performance of the data assimilation system, Q. J. Roy. Meteorol. Soc., 137, 553–597, https://doi.org/10.1002/qj.828, 2011.

Dirmeyer, P. A., Balsamo, G., Blyth, E. M., Morrison, R., and Cooper, H. M.: Land-Atmosphere Interactions Exacerbated the Drought and Heatwave Over Northern Europe During Summer 2018, AGU Adv., 2, e2020AV000283, https://doi.org/10.1029/2020AV000283, 2021.

Dole, R., Hoerling, M., Perlwitz, J., Eischeid, J., Pegion, P., Zhang, T., Quan, X.-W., Xu, T., and Murray, D.: Was there a basis for anticipating the 2010 Russian heat wave?, Geophys. Res. Lett., 38, L06702, https://doi.org/10.1029/2010GL046582, 2011.

Dole, R., Hoerling, M., Kumar, A., Eischeid, J., Perlwitz, J., Quan, X.-W., Kiladis, G., Webb, R., Murray, D., Chen, M., Wolter, K., and Zhang, T.: The making of an extreme event: putting the pieces together, B. Am. Meteorol. Soc., 95, 427–440, https://doi.org/10.1175/BAMS-D-12-00069.1, 2014.

Dong, B., Sutton, R., Shaffrey, L., and Wilcox, L.: The 2015 European heat wave, B. Am. Meteorol. Soc., 97, 57–62, https://doi.org/10.1175/BAMS-D-16-0140.1, 2016.

Döscher, R., Acosta, M., Alessandri, A., Anthoni, P., Arsouze, T., Bergman, T., Bernardello, R., Boussetta, S., Caron, L.-P., Carver, G., Castrillo, M., Catalano, F., Cvijanovic, I., Davini, P., Dekker, E., Doblas-Reyes, F. J., Docquier, D., Echevarria, P., Fladrich, U., Fuentes-Franco, R., Gröger, M., v. Hardenberg, J., Hieronymus, J., Karami, M. P., Keskinen, J.-P., Koenigk, T., Makkonen, R., Massonnet, F., Ménégoz, M., Miller, P. A., Moreno-Chamarro, E., Nieradzik, L., van Noije, T., Nolan, P., O'Donnell, D., Ollinaho, P., van den Oord, G., Ortega, P., Prims, O. T., Ramos, A., Reerink, T., Rousset, C., Ruprich-Robert, Y., Le Sager, P., Schmith, T., Schrödner, R., Serva, F., Sicardi, V., Sloth Madsen, M., Smith, B., Tian, T., Tourigny, E., Uotila, P., Vancoppenolle, M., Wang, S., Wårlind, D., Willén, U., Wyser, K., Yang, S., Yepes-Arbós, X., and Zhang, Q.: The EC-Earth3 Earth system model for the Coupled Model Intercomparison Project 6, Geosci. Model Dev., 15, 2973–3020, https://doi.org/10.5194/gmd-15-2973-2022, 2022.

Duchez, A., Frajka-Williams, E., Josey, S. A., Evans, D. G., Grist, J. P., Marsh, R., McCarthy, G. D., Sinha, B., Berry, D. I., and Hirschi, J. J.-M.: Drivers of exceptionally cold North Atlantic ocean temperatures and their link to the 2015 European heat wave, Environ. Res. Lett., 11, 074004, https://doi.org/10.1088/1748-9326/11/7/074004, 2016.

Fernandez-Granja, J. A., Casanueva, A., Bedia, J., and Fernandez, J.: Improved atmospheric circulation over Europe by the new generation of CMIP6 earth system models, Clim. Dynam., 56, 3527–3540, https://doi.org/10.1007/s00382-021-05652-9, 2021.

Fischer, E. M., Seneviratne, S. I., Vidale, P. L., Lüthi, D., and Schär, C.: Soil moisture-atmosphere interactions during the 2003 European Summer heat wave, J. Climate, 20, 5081–5099, https://doi.org/10.1175/JCLI4288.1, 2007.

Flato, G., Marotzke, J., Abiodun, B., Braconnot, P., Chou, S., Collins, W., Cox, P., Driouech, F., Emori, S., Eyring, V., Forest, C., Gleckler, P., Guilyardi, E., Jakob, C., Kattsov, V., Reason, C., and Rummukainen, M.: Evaluation of climate models, book section 9, Cambridge University Press, Cambridge, United Kingdom and New York, NY, USA, 741–866, https://doi.org/10.1017/CBO9781107415324.020, 2013.

Guillod, B. P., Orlowsky, B., Miralles, D. G., Teuling, A. J., and Seneviratne, S. I.: Reconciling spatial and temporal soil moisture effects on afternoon rainfall, Nat. Commun., 6, 6443, https://doi.org/10.1038/ncomms7443, 2015.

Harris, I., Osborn, T. J., Jones, P., and Lister, D.: Version 4 of the CRU TS monthly high-resolution gridded multivariate climate dataset, Scient. Data, 7, 109, https://doi.org/10.1038/s41597-020-0453-3, 2020.

Hauser, M., Orth, R., and Seneviratne, S. I.: Role of soil moisture versus recent climate change for the 2010 heat wave in western Russia, Geophys. Res. Lett., 43, 2819–2826, https://doi.org/10.1002/2016GL068036, 2016.

Hauser, M., Gudmundsson, L., Orth, R., Jézéquel, A., Haustein, K., Vautard, R., van Oldenborgh, G. J., Wilcox, L., and Seneviratne, S. I.: Methods and model dependency of extreme event attribution: the 2015 European drought, Earth's Future, 5, 1034–1043, https://doi.org/10.1002/2017EF000612, 2017a.

Hauser, M., Orth, R., and Seneviratne, S. I.: Investigating soil moisture–climate interactions with prescribed soil moisture experiments: An assessment with the Community Earth System Model (version 1.2), Geosci. Model Dev., 10, 1665–1677, https://doi.org/10.5194/gmd-10-1665-2017, 2017b.

Hirsch, A. L., Guillod, B. P., Seneviratne, S. I., Beyerle, U., Boysen, L. R., Brovkin, V., Davin, E. L., Doelman, J. C., Kim, H., Mitchell, D. M., Nitta, T., Shiogama, H., Sparrow, S., Stehfest, E., van Vuuren, D. P., and Wilson, S.: Biogeophysical Impacts of Land-Use Change on Climate Extremes in Low-Emission Scenarios: Results From HAPPI-Land, Earth's Future, 6, 396–409, https://doi.org/10.1002/2017EF000744, 2018.

Hirschi, M., Seneviratne, S. I., Alexandrov, V., Boberg, F., Boroneant, C., Christensen, O. B., Formayer, H., Orlowsky, B., and Stepanek, P.: Observational evidence for soil-moisture impact on hot extremes in southeastern Europe, Nat. Geosci., 4, 17–21, https://doi.org/10.1038/ngeo1032, 2011.

Hoerling, M., Eischeid, J., Kumar, A., Leung, R., Mariotti, A., Mo, K., Schubert, S. D., and Seager, R.: Causes and predictability of the 2012 Great Plains drought, B. Am. Meteorol. Soc., 95, 269–282, https://doi.org/10.1175/BAMS-D-13-00055.1, 2014.

Hope, P., Wang, G., Lim, E.-P., Hendon, H. H., and Arblaster, J. M.: What caused the record-breaking heat across Australia in October 2015?, B. Am. Meteorol. Soc., 97, 122–126, https://doi.org/10.1175/BAMS-D-16-0141.1, 2016.

Hurrell, J. W., Hack, J. J., Shea, D., Caron, J. M., and Rosinski, J.: A new sea surface temperature and sea ice boundary dataset for the Community Atmosphere Model, J. Climate, 21, 5145–5153, https://doi.org/10.1175/2008JCLI2292.1, 2008.

Hurrell, J. W., Holland, M. M., Gent, P. R., Ghan, S., Kay, J. E., Kushner, P. J., Lamarque, J.-F., Large, W. G., Lawrence, D., Lindsay, K., Lipscomb, W. H., Long, M. C., Mahowald, N., Marsh, D. R., Neale, R. B., Rasch, P., Vavrus, S., Vertenstein, M., Bader, D., Collins, W. D., Hack, J. J., Kiehl, J., and Marshall, S.: The Community Earth System Model: a framework for collaborative research, B. Am. Meteorol. Soc., 94, 1339–1360, https://doi.org/10.1175/BAMS-D-12-00121.1, 2013.

Iturbide, M., Gutiérrez, J. M., Alves, L. M., Bedia, J., Cerezo-Mota, R., Cimadevilla, E., Cofiño, A. S., Di Luca, A., Faria, S. H., Gorodetskaya, I. V., Hauser, M., Herrera, S., Hennessy, K., Hewitt, H. T., Jones, R. G., Krakovska, S., Manzanas, R., Martínez-Castro, D., Narisma, G. T., Nurhati, I. S., Pinto, I., Seneviratne, S. I., van den Hurk, B., and Vera, C. S.: An update of IPCC climate reference regions for subcontinental analysis of climate model data: Definition and aggregated datasets, Earth Syst. Sci. Data, 12, 2959–2970, https://doi.org/10.5194/essd-12-2959-2020, 2020.

Jaeger, E. B. and Seneviratne, S. I.: Impact of soil moisture-atmosphere coupling on European climate extremes and trends in a regional climate model, Clim. Dynam., 36, 1919–1939, https://doi.org/10.1007/s00382-010-0780-8, 2011.

Jeuken, A. B. M., Siegmund, P. C., Heijboer, L. C., Feichter, J., and Bengtsson, L.: On the potential of assimilating meteorological analyses in a global climate model for the purpose of model validation, J. Geophys. Res.-Atmos., 101, 16939–16950, https://doi.org/10.1029/96JD01218, 1996.

King, A. D., Karoly, D. J., Donat, M. G., and Alexander, L. V.: Climate change turns Australia's 2013 big dry into a year of record-breaking heat [in "Explaining Extremes of 2013 from a Climate Perspective"], B. Am. Meteorol. Soc., 95, 41–45, https://doi.org/10.1175/1520-0477-95.9.S1.1, 2014.

Knutti, R., Masson, D., and Gettelman, A.: Climate model genealogy: Generation CMIP5 and how we got there, Geophys. Res. Lett., 40, 1194–1199, https://doi.org/10.1002/grl.50256, 2013.

Kooperman, G. J., Pritchard, M. S., Ghan, S. J., Wang, M., Somerville, R. C. J., and Russell, L. M.: Constraining the influence of natural variability to improve estimates of global aerosol indirect effects in a nudged version of the Community Atmosphere Model 5, J. Geophys. Res.-Atmos., 117, D23204, https://doi.org/10.1029/2012JD018588, d23204, 2012.

Koster, R. D., Dirmeyer, P. A., Guo, Z., Bonan, G., Chan, E., Cox, P., Gordon, C. T., Kanae, S., Kowalczyk, E., Lawrence, D., Liu, P., Lu, C.-H., Malyshev, S., McAvaney, B., Mitchell, K., Mocko, D., Oki, T., Oleson, K., Pitman, A., Sud, Y. C., Taylor, C. M., Verseghy, D., Vasic, R., Xue, Y., and Yamada, T.: Regions of strong coupling between soil moisture and precipitation, Science, 305, 1138–1140, https://doi.org/10.1126/science.1100217, 2004.

Koster, R. D., Guo, Z., Yang, R., Dirmeyer, P. A., Mitchell, K., and Puma, M. J.: On the nature of soil mois-

ture in land surface models, J. Climate, 22, 4322–4335, https://doi.org/10.1175/2009JCLI2832.1, 2009.

Kröner, N., Kotlarski, S., Fischer, E. M., Lüthi, D., Zubler, E., and Schär, C.: Separating climate change signals into thermodynamic, lapse-rate and circulation effects: theory and application to the European summer climate, Clim. Dynam., 48, 3425–3440, https://doi.org/10.1007/s00382-016-3276-3, 2017.

Lawrence, D. M., Oleson, K. W., Flanner, M. G., Thornton, P. E., Swenson, S. C., Lawrence, P. J., Zeng, X., Yang, Z. L., Levis, S., Sakaguchi, K., Bonan, G. B., and Slater, A. G.: Parameterization improvements and functional and structural advances in version 4 of the Community Land Model, J. Adv. Model. Earth Syst., 3, M03001, https://doi.org/10.1029/2011MS00045, 2011.

Lewis, S. C. and Karoly, D. J.: Anthropogenic contributions to Australia's record summer temperatures of 2013, Geophys. Res. Lett., 40, 3705–3709, https://doi.org/10.1002/grl.50673, 2013.

Luo, F., Selten, F., Wehrli, K., Kornhuber, K., Le Sager, P., May, W., Reerink, T., Seneviratne, S. I., Shiogama, H., Tokuda, D., Kim, H., and Coumou, D.: Summertime Rossby waves in climate models: Substantial biases in surface imprint associated with small biases in upper-level circulation, Weather Clim. Dynam., 3, 905–935, https://doi.org/10.5194/wcd-3-905-2022, 2022.

Maraun, D., Shepherd, T. G., Widmann, M., Zappa, G., Walton, D., Gutiérrez, J., Hagemann, S., Richter, I., Soares, P. M. M., Hall, A., and Mearns, L. O.: Towards process-informed bias correction of climate change simulations, Nat. Clim. Change, 7, 764–773, https://doi.org/10.1038/nclimate3418, 2017.

Martius, O., Sodemann, H., Joos, H., Pfahl, S., Winschall, A., Croci-Maspoli, M., Graf, M., Madonna, E., Mueller, B., Schemm, S., Sedláček, J., Sprenger, M., and Wernli, H.: The role of upper-level dynamics and surface processes for the Pakistan flood of July 2010, Q. J. Roy. Meteorol. Soc., 139, 1780–1797, https://doi.org/10.1002/qj.2082, 2012.

Mauritsen, T., Stevens, B., Roeckner, E., Crueger, T., Esch, M., Giorgetta, M., Haak, H., Jungclaus, J., Klocke, D., Matei, D., Mikolajewicz, U., Notz, D., Pincus, R., Schmidt, H., and Tomassini, L.: Tuning the climate of a global model, J. Adv. Model. Earth Syst., 4, M00A01, https://doi.org/10.1029/2012MS000154, 2012.

Meinshausen, M., Nicholls, Z. R. J., Lewis, J., Gidden, M. J., Vogel, E., Freund, M., Beyerle, U., Gessner, C., Nauels, A., Bauer, N., Canadell, J. G., Daniel, J. S., John, A., Krummel, P. B., Luderer, G., Meinshausen, N., Montzka, S. A., Rayner, P. J., Reimann, S., Smith, S. J., van den Berg, M., Velders, G. J. M., Vollmer, M. K., and Wang, R. H. J.: The shared socioeconomic pathway (SSP) greenhouse gas concentrations and their extensions to 2500, Geosci. Model Dev., 13, 3571–3605, https://doi.org/10.5194/gmd-13-3571-2020, 2020.

Merz, B., Kuhlicke, C., Kunz, M., Pittore, M., Babeyko, A., Bresch, D. N., Domeisen, D. I. V., Feser, F., Koszalka, I., Kreibich, H., Pantillon, F., Parolai, S., Pinto, J. G., Punge, H. J., Rivalta, E., Schröter, K., Strehlow, K., Weisse, R., and Wurpts, A.: Impact forecasting to support emergency management of natural hazards, Rev. Geophys., 58, e2020RG000704, https://doi.org/10.1029/2020RG000704, 2020.

Miralles, D. G., van den Berg, M. J., Teuling, A. J., and de Jeu, R. A. M.: Soil moisture-temperature coupling: a multiscale observational analysis, Geophys. Res. Lett., 39, L21707, https://doi.org/10.1029/2012GL053703, 2012.

Miralles, D. G., Gentine, P., Seneviratne, S. I., and Teuling, A. J.: Land–atmospheric feedbacks during droughts and heatwaves: state of the science and current challenges, Ann. NY Acad. Sci., 1436, 19–35, https://doi.org/10.1111/nyas.13912, 2019.

Mitchell, D., AchutaRao, K., Allen, M. R., Bethke, I., Beyerle, U., Ciavarella, A., Forster, P. M., Fuglestvedt, J., Gillett, N., Haustein, K., Ingram, W., Iversen, T., Kharin, V., Klingaman, N., Massey, N., Fischer, E. M., Schleussner, C.-F., Scinocca, J., Seland, Ø., Shiogama, H., Shuckburgh, E., Sparrow, S., Stone, D., Uhe, P., Wallom, D., Wehner, M., and Zaaboul, R.: Half a degree additional warming, prognosis and projected impacts (HAPPI): background and experimental design, Geosci. Model Dev., 10, 571–583, https://doi.org/10.5194/gmd-10-571-2017, 2017.

Moon, H., Gudmundsson, L., and Seneviratne, S. I.: Drought persistence errors in global climate models, J. Geophys. Res.-Atmos., 123, 3483–3496, https://doi.org/10.1002/2017JD027577, 2018.

Moon, H., Guillod, B. P., Gudmundsson, L., and Seneviratne, S. I.: Soil moisture effects on afternoon precipitation occurrence in current climate models, Geophys. Res. Lett., 46, 1861–1869, https://doi.org/10.1029/2018GL080879, 2019.

Mueller, B. and Seneviratne, S. I.: Systematic land climate and evapotranspiration biases in CMIP5 simulations, Geophys. Res. Lett., 41, 128–134, https://doi.org/10.1002/2013GL058055, 2014.

Mueller, B., Hirschi, M., Jimenez, C., Ciais, P., Dirmeyer, P. A., Dolman, A. J., Fisher, J. B., Jung, M., Ludwig, F., Maignan, F., Miralles, D. G., McCabe, M. F., Reichstein, M., Sheffield, J., Wang, K., Wood, E. F., Zhang, Y., and Seneviratne, S. I.: Benchmark products for land evapotranspiration: LandFluxEVAL multi-data set synthesis, Hydrol. Earth Syst. Sci., 17, 3707–3720, https://doi.org/10.5194/hess-17-3707-2013, 2013.

Neale, R. B., Chen, C.-C., Gettelman, A., Lauritzen, P. H., Park, S., Williamson, D. L., Conley, A. J., Garcia, R., Kinnison, D., Lamarque, J.-F., Marsh, D., Mills, M., Smith, A. K., Tilmes, S., Vitt, F., Morrison, H., Cameron-Smith, P., Collins, W. D., Iacono, M. J., Easter, R. C., Ghan, S. J., Liu, X., Rasch, P. J., and Taylor, M. A.: Description of the NCAR Community Atmosphere Model (CAM 5.0), Technical report, National Center for Atmospheric Research, Boulder, Colorado, https://www.cesm.ucar.edu/models/cesm1.0/cam/docs/description/cam5_desc.pdf (last access: 26 July 2022), 2012.

NOAA Climate Prediction Center: Historical El Niño/La Niña episodes (1950–present) based on the Oceanic Niño Index, https://origin.cpc.ncep.noaa.gov/products/analysis_monitoring/ensostuff/ONI_v5.php, last access: 15 February 2022.

Oleson, K. W., Lawrence, D. M., Bonan, G. B., Flanner, M. G., Kluzek, E., Lawrence, P. J., Levis, S., Swenson, S. C., Thornton, P. E., Dai, A., Decker, M., Dickinson, R., Feddema, J., Heald, C. L., Hoffman, F., Lamarque, J.-F., Mahowald, N., Niu, G.-Y., Qian, T., Randerson, J., Running, S., Sakaguchi, K., Slater, A., Stöckli, R., Wang, A., Yang, Z.-L., Zeng, X., and Zeng, X.: Technical description of version 4.0 of the Community Land Model (CLM), Technical report, National Center for Atmospheric Research, Boulder, Colorado, https://www.cesm.ucar.edu/models/cesm2/land/CLM4_Tech_Note.pdf (last access: 26 July 2022), 2010.

Orth, R., Zscheischler, J., and Seneviratne, S. I.: Record dry summer in 2015 challenges precipitation projections in Central Europe, Scient. Rep., 6, 28334, https://doi.org/10.1038/srep28334, 2016.

PaiMazumder, D. and Done, J. M.: Potential predictability sources of the 2012 U.S. drought in observations and a regional model ensemble, J. Geophys. Res.-Atmos., 121, 12581–12592, https://doi.org/10.1002/2016JD025322, 2016.

Petch, J. C., Short, C. J., Best, M. J., McCarthy, M., Lewis, H. W., Vosper, S. B., and Weeks, M.: Sensitivity of the 2018 UK summer heatwave to local sea temperatures and soil moisture, Atmos. Sci. Lett., 21, e948, https://doi.org/10.1002/asl.948, 2020.

Pfahl, S., O'Gorman, P. A., and Fischer, E. M.: Understanding the regional pattern of projected future changes in extreme precipitation, Nat. Clim. Change, 7, 423–427, https://doi.org/10.1038/nclimate3287, 2017.

Power, S. B. and Delage, F. P. D.: Setting and smashing extreme temperature records over the coming century, Nat. Clim. Change, 9, 529–534, https://doi.org/10.1038/s41558-019-0498-5, 2019.

Quesada, B., Vautard, R., Yiou, P., Hirschi, M., and Seneviratne, S. I.: Asymmetric European summer heat predictability from wet and dry southern winters and springs, Nat. Clim. Change, 2, 736–741, https://doi.org/10.1038/nclimate1536, 2012.

Rahmstorf, S. and Coumou, D.: Increase of extreme events in a warming world, P. Natl. Acad. Sci. USA, 108, 17905–17909, https://doi.org/10.1073/pnas.1101766108, 2011.

Rayner, N. A., Parker, D. E., Horton, E. B., Folland, C. K., Alexander, L. V., Rowell, D. P., Kent, E. C., and Kaplan, A.: Global analyses of sea surface temperature, sea ice, and night marine air temperature since the late nineteenth century, J. Geophys. Res.-Atmos., 108, 4407, https://doi.org/10.1029/2002JD002670, 2003.

Rossow, W. B. and Schiffer, R. A.: Advances in Understanding Clouds from ISCCP, B. Am. Meteorol. Soc., 80, 2261–2288, https://doi.org/10.1175/1520-0477(1999)080<2261:AIUCFI>2.0.CO;2, 1999.

Santanello, J. A., Dirmeyer, P. A., Ferguson, C. R., Findell, K. L., Tawfik, A. B., Berg, A., Ek, M., Gentine, P., Guillod, B. P., van Heerwaarden, C., Roundy, J., and Wulfmeyer, V.: Land-atmosphere interactions: the LoCo perspective, B. Am. Meteorol. Soc., 99, 1253–1272, https://doi.org/10.1175/BAMS-D-17-0001.1, 2018.

Seneviratne, S. I., Lüthi, D., Litschi, M., and Schär, C.: Land-atmosphere coupling and climate change in Europe, Nature, 443, 205–209, https://doi.org/10.1038/nature05095, 2006.

Seneviratne, S. I., Corti, T., Davin, E. L., Hirschi, M., Jaeger, E. B., Lehner, I., Orlowsky, B., and Teuling, A. J.: Investigating soil moisture-climate interactions in a changing climate: A review, Earth-Sci. Rev., 99, 125–161, https://doi.org/10.1016/j.earscirev.2010.02.004, 2010.

Seneviratne, S. I., Nicholls, N., Easterling, D., Goodess, C. M., Kanae, S., Kossin, J., Luo, Y., Marengo, J., Innes, K. M., Rahimi, M., Reichstein, M., Sorteberg, A., Vera, C., Zhang, X., Rusticucci, M., Semenov, V., Alexander, L. V., Allen, S., Benito, G., Cavazos, T., Clague, J., Conway, D., Della-Marta, P. M., Gerber, M., Gong, S., Goswami, B. N., Hemer, M., Huggel, C., den Hurk, B. V., Kharin, V. V., Kitoh, A., Tank, A. M. G. K., Li, G., Mason, S., Guire, W. M., Oldenborgh, G. J. V., Orlowsky, B., Smith, S., Thiaw, W., Velegrakis, A., Yiou, P., Zhang, T., Zhou, T., and Zwiers, F. W.: Changes in climate extremes and their impacts on the natural physical environment, in: Managing the Risks of Extreme Events and Disasters to Advance Climate Change Adaptation, edited by: Field, C. B., Barros, V., Stocker, T. F., and Dahe, Q., Cambridge University Press, Cambridge, 109–230, https://doi.org/10.1017/CBO9781139177245.006, 2012.

Seneviratne, S. I., Donat, M. G., Mueller, B., and Alexander, L. V.: No pause in the increase of hot temperature extremes, Nat. Clim. Change, 4, 161–163, https://doi.org/10.1038/nclimate2145, 2014.

Shepherd, T. G.: Atmospheric circulation as a source of uncertainty in climate change projections, Nat. Geosci., 7, 703–708, https://doi.org/10.1038/ngeo2253, 2014.

Shiogama, H., Watanabe, M., Imada, Y., Mori, M., Ishii, M., and Kimoto, M.: An event attribution of the 2010 drouwght in the South Amazon region using the MIROC5 model, Atmos. Sci. Lett., 14, 170–175, https://doi.org/10.1002/asl2.435, 2013.

Shiogama, H., Imada, Y., Mori, M., Mizuta, R., Stone, D., Yoshida, K., Arakawa, O., Ikeda, M., Takahashi, C., Arai, M., Ishii, M., Watanabe, M., and Kimoto, M.: Attributing historical changes in probabilities of record-breaking daily temperature and precipitation extreme events, Scient. Onl. Lett. Atmos., 12, 225–231, 2016.

Shiogama, H., Hasegawa, T., Fujimori, S., Murakami, D., Takahashi, K., Tanaka, K., Emori, S., Kubota, I., Abe, M., Imada, Y., Watanabe, M., Mitchell, D., Schaller, N., Sillmann, J., Fischer, E. M., Scinocca, J. F., Bethke, I., Lierhammer, L., Takakura, J., Trautmann, T., Döll, P., Ostberg, S., Schmied, H. M., Saeed, F., and Schleussner, C.-F.: Limiting global warming to 1.5 °C will lower increases in inequalities of four hazard indicators of climate change, Environ. Res. Lett., 14, 124022, https://doi.org/10.1088/1748-9326/ab5256, 2019.

Sillmann, J., Kharin, V. V., Zwiers, F. W., Zhang, X., and Bronaugh, D.: Climate extremes indices in the CMIP5 multimodel ensemble: Part 2. Future climate projections, J. Geophys. Res.-Atmos., 118, 2473–2493, https://doi.org/10.1002/jgrd.50188, 2013.

Suarez-Gutierrez, L., Müller, W. A., Li, C., and Marotzke, J.: Dynamical and thermodynamical drivers of variability in European summer heat extremes, Clim. Dynam., 54, 4351–4366, https://doi.org/10.1007/s00382-020-05233-2, 2020.

Takata, K., Emori, S., and Watanabe, T.: Development of the minimal advanced treatments of surface interaction and runoff, Global Planet. Change, 38, 209–222, https://doi.org/10.1016/S0921-8181(03)00030-4, 2003.

Trenberth, K. E. and Fasullo, J. T.: Climate extremes and climate change: the Russian heat wave and other climate extremes of 2010, J. Geophys. Res.-Atmos., 117, D17103, https://doi.org/10.1029/2012JD018020, 2012.

Trenberth, K. E., Fasullo, J. T., and Shepherd, T. G.: Attribution of climate extreme events, Nat. Clim. Change, 5, 725–730, https://doi.org/10.1038/nclimate2657, 2015.

Turner, J., Bracegirdle, T. J., Phillips, T., Marshall, G. J., and Hosking, J. S.: An initial assessment of Antarctic sea ice extent in the CMIP5 models, J. Climate, 26, 1473–1484, https://doi.org/10.1175/JCLI-D-12-00068.1, 2013.

van der Ent, R. J., Savenije, H. H. G., Schaefli, B., and Steele-Dunne, S. C.: Origin and fate of atmospheric moisture over continents, Water Resour. Res., 46, W09525, https://doi.org/10.1029/2010WR009127, 2010.

van Vuuren, D. P., Edmonds, J., Kainuma, M., Riahi, K., Thomson, A., Hibbard, K., Hurtt, G. C., Kram, T., Krey, V., Lamarque, J.-F., Masui, T., Meinshausen, M., Nakicenovic, N., Smith, S. J., and Rose, S. K.: The representative concentration pathways: An overview, Climatic Change, 109, 5–31, https://doi.org/10.1007/s10584-011-0148-z, 2011.

Vautard, R., Yiou, P., Otto, F., Stott, P., Christidis, N., van Oldenborgh, G. J., and Schaller, N.: Attribution of human-induced dynamical and thermodynamical contributions in extreme weather events, Environ. Res. Lett., 11, 114009, https://doi.org/10.1088/1748-9326/11/11/114009, 2016.

Wang, C., Zhang, L., Lee, S.-K., Wu, L., and Mechoso, C. R.: A global perspective on CMIP5 climate model biases, Nat. Clim. Change, 4, 201–205, https://doi.org/10.1038/nclimate2118, 2014.

Wang, G., Hope, P., Lim, E.-P., Hendon, H. H., and Arblaster, J. M.: Three methods for the attribution of extreme weather and climate events, Research Report 018, Bureau of Meteorology, http://www.bom.gov.au/research/publications/researchreports/BRR-018.pdf (last access: 26 July 2022), 2016.

Wang, H., Schubert, S. D., Koster, R., Ham, Y.-G., and Suarez, M.: On the role of SST forcing in the 2011 and 2012 extreme U.S. heat and drought: a study in contrasts, J. Hydrometeorol., 15, 1255–1273, https://doi.org/10.1175/JHM-D-13-069.1, 2014.

Watanabe, M., Suzuki, T., O'ishi, R., Komuro, Y., Watanabe, S., Emori, S., Takemura, T., Chikira, M., Ogura, T., Sekiguchi, M., Takata, K., Yamazaki, D., Yokohata, T., Nozawa, T., Hasumi, H., Tatebe, H., and Kimoto, M.: Improved climate simulation by MIROC5: mean states, variability, and climate sensitivity, J. Climate, 23, 6312–6335, https://doi.org/10.1175/2010JCLI3679.1, 2010.

Wehrli, K., Guillod, B. P., Hauser, M., Leclair, M., and Seneviratne, S. I.: Assessing the dynamic versus thermodynamic origin of climate model biases, Geophys. Res. Lett., 45, 8471–8479, https://doi.org/10.1029/2018GL079220, 2018.

Wehrli, K., Guillod, B. P., Hauser, M., Leclair, M., and Seneviratne, S. I.: Identifying key driving processes of major recent heat waves, J. Geophys. Res.-Atmos., 124, 11746–11765, https://doi.org/10.1029/2019JD030635, 2019.

Wehrli, K., Hauser, M., and Seneviratne, S. I.: Storylines of the 2018 Northern Hemisphere heatwave at pre-industrial and higher global warming levels, Earth Syst. Dynam., 11, 855–873, https://doi.org/10.5194/esd-11-855-2020, 2020.

Wehrli, K., Luo, F., Hauser, M., Shiogama, H., Tokuda, D., Kim, H., Coumou, D., May, W., Le Sager, P., Selten, F., Martius, O., Vautard, R., and Seneviratne, S. I.: The ExtremeX global climate model experiment data, ETH Zurich [data set], https://data.iac.ethz.ch/Wehrli_et_al_2022_ExtremeX/, last access: 20 August 2022.

Zappa, G., Shaffrey, L. C., and Hodges, K. I.: The ability of CMIP5 models to simulate North Atlantic extratropical cyclones, J. Climate, 26, 5379–5396, https://doi.org/10.1175/JCLI-D-12-00501.1, 2013.

Zappa, G., Hoskins, B. J., and Shepherd, T. G.: The dependence of wintertime Mediterranean precipitation on the atmospheric circulation response to climate change, Environ. Res. Lett., 10, 104012, https://doi.org/10.1088/1748-9326/10/10/104012, 2015.

Ziese, M., Rauthe-Schöch, A., Becker, A., Finger, P., Meyer-Christoffer, A., and Schneider, U.: GPCC Full Data Daily Version.2018 at 1.0°: daily land-surface precipitation from rain-gauges built on GTS-based and historic data, DWD, https://doi.org/10.5676/dwd_gpcc/fd_d_v2018_100, 2018.